Human Molecular Genetics, 2016, Vol. 25, No. 6 1100–1115

doi: 10.1093/hmg/ddv633
Advance Access Publication Date: 5 January 2016
Original Article

ORIGINAL ARTICLE

α-Synuclein interferes with the ESCRT-III complex contributing to the pathogenesis of Lewy body disease

Brian Spencer[1], Changyoun Kim[1,3], Tania Gonzalez[1], Alejandro Bisquertt[1], Christina Patrick[1], Edward Rockenstein[1], Anthony Adame[1], Seung-Jae Lee[3], Paula Desplats[1] and Eliezer Masliah[1,2,*]

[1]Department of Neuroscience and [2]Department of Pathology, University of California, San Diego, San Diego, CA 92103, USA and [3]Department of Medicine, College of Medicine, Seoul National University, Seoul 110-799, Korea

*To whom correspondence should be addressed at: Department of Neuroscience, University of California San Diego, San Diego, CA 92093-0624, USA. Tel: +1 858 5348992; Fax: +1 858 5346232; Email: emasliah@ucsd.edu

Abstract

α-Synuclein (α-syn) has been implicated in neurological disorders with parkinsonism, including Parkinson's disease and Dementia with Lewy body. Recent studies have shown α-syn oligomers released from neurons can propagate from cell-to-cell in a prion-like fashion exacerbating neurodegeneration. In this study, we examined the role of the endosomal sorting complex required for transport (ESCRT) pathway on the propagation of α-syn. α-syn, which is transported via the ESCRT pathway through multivesicular bodies for degradation, can also target the degradation of the ESCRT protein-charged multivesicular body protein (CHMP2B), thus generating a roadblock of endocytosed α-syn. Disruption of the ESCRT transport system also resulted in increased exocytosis of α-syn thus potentially increasing cell-to-cell propagation of synuclein. Conversely, delivery of a lentiviral vector overexpressing CHMP2B rescued the neurodegeneration in α-syn transgenic mice. Better understanding of the mechanisms of intracellular trafficking of α-syn might be important for understanding the pathogenesis and developing new treatments for synucleinopathies.

Introduction

A number of neurodegenerative disorders of the aging population are characterized by progressive accumulation of aggregated proteins (e.g. α-synuclein (α-syn), Aβ, SOD-1 and tau) inside of cells (1). Moreover, recent studies suggest that many of these protein aggregates might propagate from cell-to-cell contributing to the hierarchical spreading of the pathology throughout interconnected circuitries in the CNS (2). α-syn a chaperone synaptic protein involved in neurotransmitter release (3) has been identified as the major protein accumulating and disseminating in patients with Parkinson's disease (PD) and dementia with Lewy body (DLB) (4–7). Although mechanisms for the release and uptake of α-syn oligomers have been examined in some detail (8,9), the intracellular trafficking and fate of the endocytosed α-syn and other protein aggregates in the recipient cells has not been sufficiently explored. It is not clear what happens and how the protein is targeted for seeding and/or clearance in the new cell.

The endosomal sorting complex required for transport (ESCRT) comprises a set of five families of proteins involved in the sorting and trafficking of proteins from the endosome to the lysosome via the multivesicular bodies (MVBs) (10–12) ultimately resulting in clearance and degradation of the MVB cargo. The ESCRTs act sequentially to traffic endosomal cargoes to the MVB, thus playing an important role in targeting endocytosed proteins for autophagy-directed degradation. Mammalian ESCRT-III proteins are unique among the families of ESCRT members in their ability to perform membrane remodeling by inducing cell invagination away from cell cytoplasm. This allows the formation of the MVB. Mammalian members of the ESCRT-III family are referred to as charged multivesicular body proteins (CHMPs) (reviewed in (10)).

Received: August 14, 2015. **Revised:** December 8, 2015. **Accepted:** December 30, 2015

The CHMP proteins have received considerable attention recently for their potential role in autophagy (13) and neurodegenerative disorders. For example, mutations in *CHMP2B* have been linked to familial forms of frontotemporal dementia (FTD-3) (14,15), amyotrophic lateral sclerosis (ALS) (16,17) and early onset Alzheimer's disease (18), and mutations in *CHMP2B* have been shown to result in defective autophagy (19,20).

In this study, we examined the role of the ESCRT endocytosis/MVB pathway in the cell-to-cell spread of α-syn. We found that extracellular α-syn is endocytosed by the ESCRT pathway and targeted for degradation by autophagy through the MVBs. The ESCRT-III protein, CHMP2B, plays a pivotal role in the trafficking of the endocytosed α-syn. Remarkably, in patients with DLB and in α-syn tg mice, levels of CHMP2B and CHMP3 were reduced (while CHMP4B/C were increased). Delivery via gene therapy of *CHMP2B*, in cell-based models and in α-syn tg mice alleviated this block and reduced the intracellular accumulation of α-syn reversing the α-syn-induced neuropathology. Thus, intracellular α-syn aggregates can interfere with and target the ESCRT component CHMP2B for degradation by autophagy thereby decreasing the degradation of endocytosed extracellular α-syn leading to accumulation of intraneuronal propagated α-syn and neurodegeneration.

Results

Extracellular α-syn is endocytosed and targeted to MVBs

Propagating α-syn is one pathway for neuronal pathology to spread in synucleinopathies (8). In order to examine the mechanism for uptake and trafficking of extracellular α-syn, we generated an *in vitro* co-culture system. In this system, two populations of cells are separated by a 0.4 µm filter membrane allowing only proteins and small molecules to passage between the two chambers containing the two separate populations of cells. In the top chamber, cells (from B103 neuroblastoma cell line) previously infected with the lentivector (LV) are overexpressing α-syn representing the 'donor cells'. In the bottom chamber, cells derived from the same line are grown on coverslips and represent the 'acceptor cells' (Fig. 1A and B). Time course analysis of α-syn in this system showed a rapid accumulation of α-syn in the media representing the extracellular α-syn and rapid uptake by the acceptor cells (Fig. 1C). To characterize the α-syn produced by the donor cells and the extracellular α-syn uptaken by the acceptor cells, immunoblot and immunocytochemical analysis was performed (Supplementary Material, Fig. S1). Both with a monoclonal and a polyclonal antibody against α-syn western blot analysis with SDS-PAGE gels showed that in the neuronal B103 cells

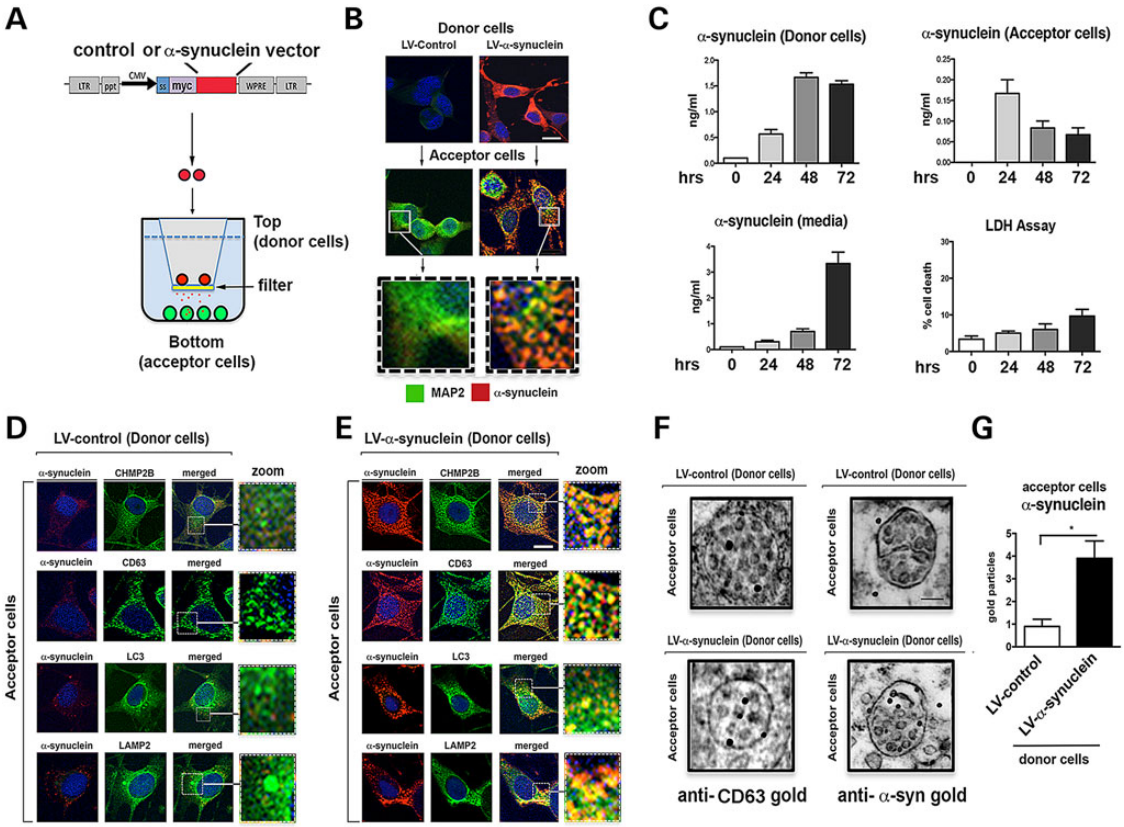

Figure 1. Endocytosed α-syn is targeted to the MVB in an *in vitro* cell-to-cell transmission assay. (**A**) An *in vitro* neuronal co-culture system was devised to mimic the propagation of α-syn. B103 neuronal 'donor cells' infected with LV-*α-syn* or LV-control (red) were plated in cell culture inserts containing a 0.4 µm membrane. B103 neuronal 'acceptor cells' were plated on coverslips. (**B**) Immunohistochemistry showing α-syn protein (red) from the donor cells was secreted and taken up by acceptor cells with the neuronal protein MAP2 (green). Scale bar = 15 µm. (**C**) Time course of α-syn expression from the donor cells, secretion into the media, uptake by the acceptor cells and LDH release assay for cell death of donor cells ($n = 4$ wells for each assay). Immunohistochemistry of co-culture with donor cells infected with (**D**) LV-control or (**E**) LV-*α-syn*. Scale bar = 15 µm. Coverslips were stained for α-syn (red) and CHMP2B, CD63, LC3 or LAMP2 (green) as well as nuclei (DAPI, blue) ($n = 3$ wells for each experiment). (**F**) Electron microscopy of acceptor cells incubated with donor cells infected with LV-control or LV-*α-syn* stained with gold particle labeled anti-CD63 or anti-α-syn. Scale bar = 1 µm. (**G**) Quantitation of gold particles per multivesicular body ($n = 3$ wells for each experiment). *Statistical significance $P < 0.05$ compared with LV-control-infected cells. One-way ANOVA with *post hoc* Tukey–Krammer.

infected with LV-α-syn displayed a band at 14 kDa corresponding to the monomer as well higher MW bands at 42 and 70 kDa corresponding to the multimers (Supplementary Material, Fig. S1A and B), in the media a weak band corresponding to the monomer was identified as well as additional MW bands that appear as a smear (Supplementary Material, Fig. S1A and B). Likewise, in the native gels, a band corresponding to monomeric α-syn was identified as well as multiple bands with a smear appearance corresponding to α-syn multimers (Supplementary Material, Fig. S1A and B). Further corroboration was performed by immunocytochemistry utilizing the SYN-1 antibody that identifies monomers and multimers of α-syn and the 5G4 antibody that favors recognizing aggregated α-syn. As expected, donor cells infected with LV-α-syn displayed strong SYN-1 and 5G4 immunoreactivity (Supplementary Material, Fig. S1C). Likewise, acceptor cells showed strong SYN-1 and 5G4 immunoreactivity (Supplementary Material, Fig. S1D). These results support the notion that LV-α-syn-infected donor cells express and secrete both monomeric and aggregated α-syn that is readily uptaken by the acceptor cells. This is consistent with our previous studies showing that extracellular α-syn is aggregated (21). The release of α-syn did not appear to be due to increased cell death (Fig. 1C). Acceptor cells showed a gradual decrease in accumulation of α-syn over the course of the experiment suggesting a degradation pathway for α-syn (Fig. 1C). Based on this time course, cells were co-cultured together for 24 h prior to analysis.

Compared with donor cells infected with the LV-control vector (Fig. 1D and Supplementary Material, Fig. S1), in chambers where the donor cells were infected with LV-α-*syn*, the acceptor cells showed accumulation of α-syn after 24 h. By confocal microscopy, this internalized α-syn strongly co-localized within granular intracellular structures with markers of the ESCRT pathway (CHMP2B), MVBs (CD63), autophagosomes (LC3) and lysosomes (LAMP2) (Fig. 1E). Combined immunogold and electron microscopy confirmed that compared with the controls, in the acceptor cells (where the donors were infected with LV-α-*syn*) the MVBs which by immunogold were CD63 positive, displayed abundant gold particles representing α-syn (Fig. 1F and G). This suggests that the extracellular α-syn is endocytosed via the ESCRT pathway and is targeted for degradation with lysosomes.

To further determine if the ESCRT pathway was required for endocytosis/degradation of extracellular α-syn, acceptor cells were infected with LVs either overexpressing (LV-*CHMP2B*) or downregulating (LV-sh*CHMP2B*) the CHMP2B protein (Supplementary Material, Fig. S2), a component of the ESCRT-III complex (Fig. 2A and B). Overexpression of CHMP2B in acceptor cells resulted in a reduced accumulation of the internalized α-syn in the acceptor cells (Fig. 2C and D). In contrast, downregulation of CHMP2B (LV-sh*CHMP2B*) resulted in a disruption in the internalization of extracellular of α-syn with extracellular α-syn accumulating in the pericellular region and with some cells lacking any endocytosed α-syn (Fig. 2E and F and Supplementary Material, Fig. S3). To verify that the α-syn observed in the acceptor cells was from the donor cells, we performed similar experiments with the LV-α-*syn*-*myc* vector and immunostained for the c-myc epitope tag (Supplementary Material, Fig. S4A). These results were confirmed in primary mouse cortical neurons (Supplementary Material, Fig. S4B).

To determine if the effects of CHMP2B were specific, we examined the effect of downregulating CHMP2A or CHMP6 through transfection of siRNA along with co-culture with the α-syn-expressing cells. Transfection of siCHMP2A did not appear to have any effect on the subcellular localization or accumulation of α-syn (Fig. 2G and H), whereas downregulation of CHMP6 reduced α-syn accumulation and increased pericellular accumulation of α-syn (Fig. 2I and J) similar to the effect of CHMP2B.

Because overexpression of CHMP2B resulted in reduced intracellular accumulation of α-syn this could be the result of an increase in clearance or a decrease in endocytosis of α-syn. To further investigate the mechanisms involved, we combined the co-culture system with pharmacological compounds that block or stimulate autophagosome/lysosome formation. We have previously shown that treatment with bafilomycin A1 (BafA1) increases the intracellular accumulation of α-syn and treatment with an activator of autophagy, rapamycin, decreases intracellular accumulation of α-syn (22,23).

As expected, compared with controls, acceptor cells overexpressing CHMP2B rapidly cleared the internalized α-syn (Fig. 3A–C and G). In contrast, serum starvation or treatment with BafA1 resulted in reduced clearance and increased accumulation of α-syn in the intracellular compartment, whereas treatment with rapamycin increased the degradation of α-syn and reduced the intracellular accumulation of α-syn (Fig. 3A–C, G and Supplementary Material, Fig. S5A–D). In contrast, acceptor cells infected with the LV-sh*CHMP2B* and serum-starved or treated with BafA1 or rapamycin showed no effects on the accumulation or clearance of α-syn as would be expected if the degradation of α-syn by autophagosomes is downstream of the ESCRT-mediated MVB formation (Fig. 3D–F, H and Supplementary Material, Fig. S5A–D). To determine if α-syn was endocytosed in a clathrin-dependent mechanism, cells were treated with the dynamin GTPase inhibitor Dynasore prior to exposure with exogenous α-syn. Treatment of the B103 neuronal cells with Dynasore prevented internalization of α-syn suggested that endocytosis occurs through a clathrin-dependent pathway (Supplementary Material, Fig. S5E and F).

Alterations of ESCRT proteins in the cells internalizing α-syn affect the accumulation, localization and degradation of α-syn. However, the ESCRT pathway could also affect the exocytosis of α-syn either as a secreted protein or as a microvesicle. To determine, if CHMP2B could affect the release of α-syn, then neuronal cells were infected with LVs expressing α-syn and either CHMP2B or siCHMP2B in a co-culture system where the acceptor cells were uninfected (Fig. 4A). Uninfected acceptor cells endocytosed α-syn when expressed from the donor cells either alone or with CHMP2B with no difference (Fig. 4B and C). In contrast, downregulation of CHMP2B in the donor cells appeared to increase the uptake of α-syn by the acceptor cells (Fig. 4B and C). Analysis of α-syn by ELISA showed that in the media secreted by LV-α-syn, levels of α-syn were higher compared with control and that knockdown of CHMP2B in donor cells resulted in even higher levels of α-syn in the media (Fig. 4D). This suggests that downregulated CHMP2B in the donor cells affected their intracellular capacity to clear α-syn leading to greater release of α-syn in the media, which in turn translated to higher levels of transmission into the donor cells in the bottom.

Thus, the model proposed for uptake of extracellular α-syn involves the import via the ESCRT-mediated endosomal pathway to the MVBs leading to the autophagosome degradation pathway (Fig. 3I and J). Overexpression of CHMP2B increases the transport of the endocytosed α-syn to the autophagosome and thus degradation (Fig. 3I) and conversely, downregulation of CHMP2B blocks the transport of newly internalized α-syn to the autophagosome leading to an accumulation in the pericellular region (Fig. 3J). Inhibition of the autophagy pathway by treatment with BafA1 blocks the degradation of α-syn leading to intracellular accumulation, regardless of levels of CHMP2B, because the autophagosome is downstream of the ESCRT pathway (Fig. 3J).

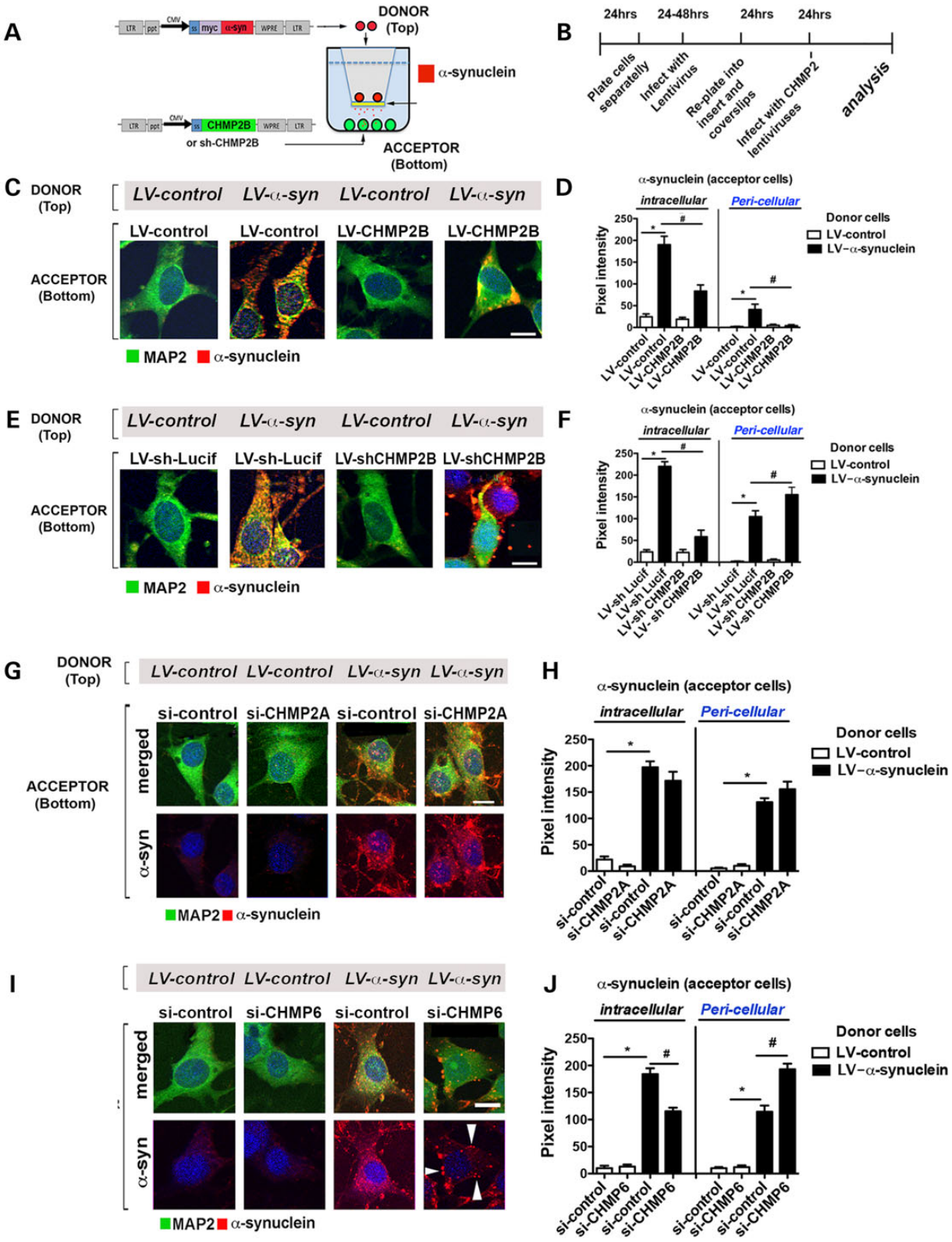

Figure 2. CHMP2B is involved in the transport of endocytosed α-syn to the MVB in an *in vitro* cell-to-cell transmission assay. (**A**) An *in vitro* neuronal co-culture system with B103 neuronal 'donor cells' infected with LV-*α-syn* or LV-control (red). B103 neuronal 'acceptor cells' infected with LV-*CHMP2B*, LV-control, LV-sh*CHMP2B*, LV-sh*Lucif* or transfected with si-CHMP2A, si-CHMP6 or si-control were plated on coverslips. (**B**) Timeline indicating infection, co-culture and analysis protocol for the experiment. (**C**) Immunohistochemistry of acceptor cells infected with LV-control or LV-*CHMP2B* co-cultured with donor cells infected with LV-control or LV-*α-syn*. Coverslips were stained for α-syn (red) and MAP2 (green) as well as nuclei (DAPI, blue). (**D**) Coverslips were analyzed to determine levels of α-syn immunoreactivity expressed as pixel intensity. (**E**) Immunohistochemistry of acceptor cells infected with LV-sh*Lucif* or LV-sh*CHMP2B* co-cultured with donor cells infected with LV-control or LV-*α-syn*. Coverslips were stained for α-syn (red) and MAP2 (green) as well as nuclei (DAPI, blue). (**F**) Coverslips were analyzed to determine levels of α-syn immunoreactivity expressed as pixel intensity. (**G**) Immunohistochemistry of acceptor cells (bottom) transfected with si-control or si-CHMP2A and co-cultured with donor cells (top)

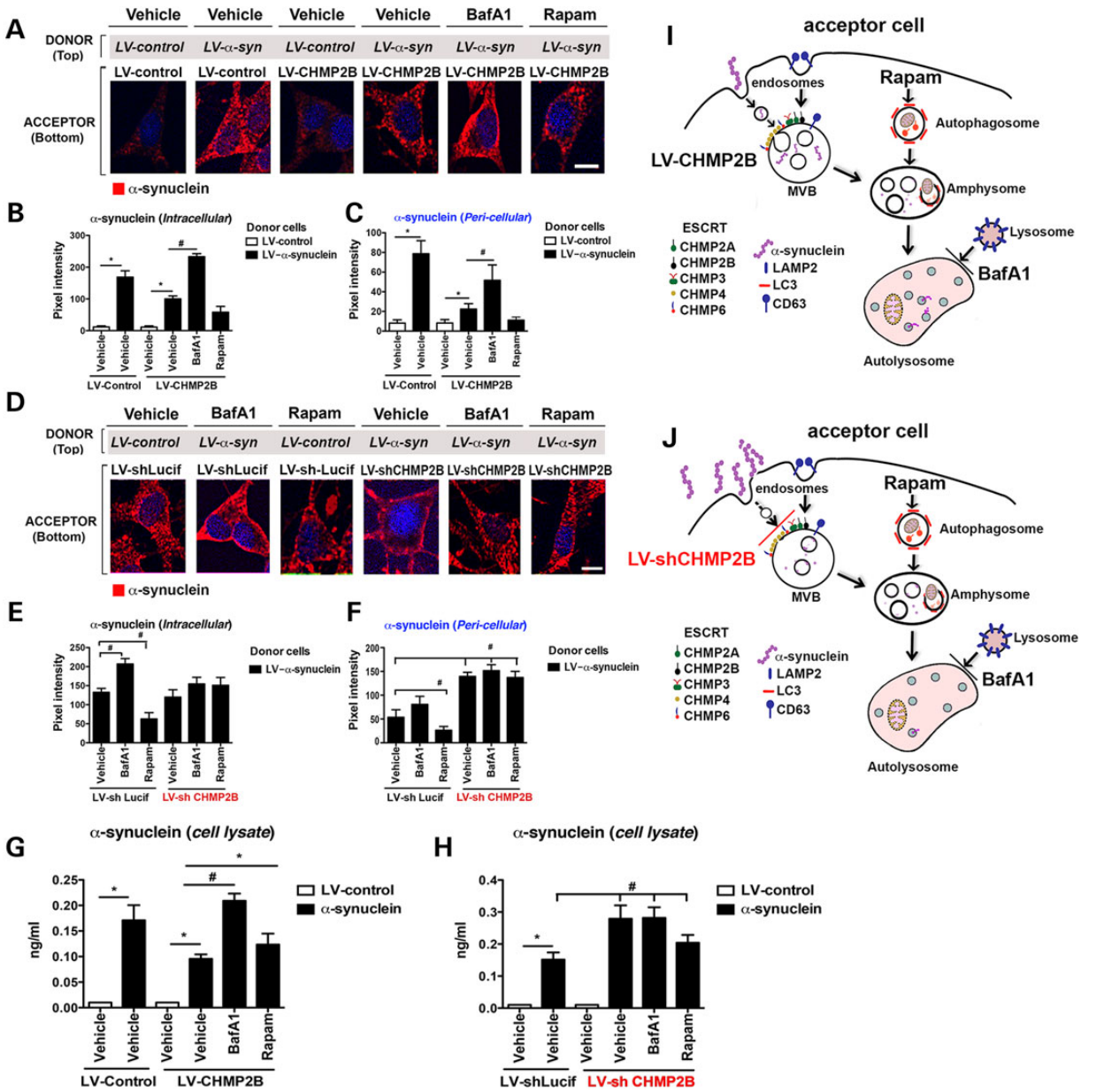

Figure 3. Endocytosed α-syn is transported to the autophagosome for degradation in an ESCRT-III-dependent manner. (**A**) Immunohistochemistry of acceptor cells infected with LV-control or LV-*CHMP2B* co-cultured with donor cells infected with LV-control or LV-*α-syn*. Cultures were then treated with BafA1, Rapamycin (Rapam) or Vehicle. Coverslips were stained for α-syn (red) and nuclei (DAPI, blue). (**B** and **C**) Coverslips were analyzed to determine levels of α-syn immunoreactivity expressed as pixel intensity. (**D**) Immunohistochemistry of acceptor cells infected with LV-sh*CHMP2B* or LV-sh*Lucif* co-cultured with donor cells infected with LV-*α-syn*. Cultures were then treated with Baf, Rapam or Vehicle. Coverslips were stained for α-syn (red) and nuclei (DAPI, blue). (**E** and **F**) Coverslips were analyzed to determine levels of α-syn immunoreactivity expressed as pixel intensity. (**G** and **H**) Lysates from acceptor cells were assayed by electrochemical α-syn assay. (**I**) Model of the effects of CHMP2B overexpression on α-syn autophagy degradation. (**J**) Model of the effects of CHMP2B downregulation on α-syn autophagy degradation. *Indicates statistical significance $P < 0.05$ compared with vehicle treatment with LV-control-infected donor cells. #Statistical significance $P < 0.05$ compared with vehicle treatment with LV-α-syn-infected donor cells. One-way ANOVA with *post hoc* Tukey–Krammer ($n = 3$ experiments per group).

infected with LV-control or LV-*α-syn*. Coverslips were immunostained for α-syn (red) and MAP2 (green) as well as nuclei (DAPI, blue). Panels are presented as merged and split image for α-syn (red). (**H**) Coverslips were analyzed with ImageJ to determine levels of α-syn immunoreactivity expressed as pixel intensity in the intracellular and pericellular compartments. (**I**) Immunohistochemical analysis of acceptor cells (bottom) transfected with si-control or si-CHMP6 and co-cultured with donor cells (top) infected with LV-control or LV-*α-syn*. Coverslips were immunostained for α-syn (red) and MAP2 (green) as well as nuclei (DAPI, blue). (**J**) Coverslips were analyzed to determine levels of α-syn immunoreactivity expressed as pixel intensity. Scale bar = 15 µm. *Statistical significance $P < 0.05$ compared with co-culture with LV-control-infected donor cells. #Statistical significance $P < 0.05$ compared with LV-control or LV-sh*Lucif* infected or si-control transfected acceptor cells. One-way ANOVA with *post hoc* Tukey–Krammer ($n = 3$ wells for each experiment).

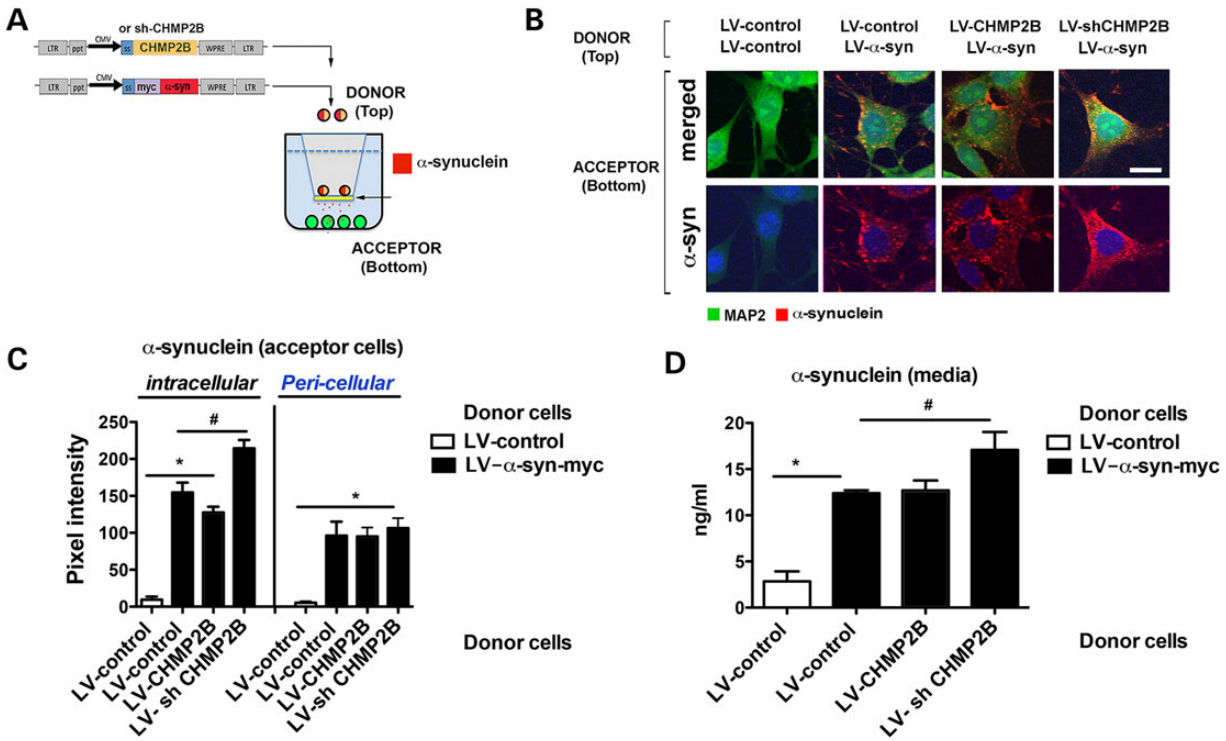

Figure 4. Effects of CHMP2B on cell-to-cell transmission of α-syn when added to donor cells. (**A**) The *in vitro* co-culture system was used with donor neuronal cell line B103 (top) infected with both LV-control or LV-*α-syn* and LV-*CHMP2B* or LV-sh*CHMP2B*. (**B**) Uninfected acceptor neuronal cell line B103 (bottom) were examined by immunohistochemistry for MAP2 (green), α-syn (red) and nuclei (DAPI, blue). Panels are presented as merged and split image for α-syn (red). (**C**) Neuronal cells were analyzed with ImageJ to determine levels of α-syn immunoreactivity expressed as pixel intensity. (**D**) Supernatant from the acceptor cell chamber was assayed by electrochemical assay for α-syn. *Indicates statistical significance $P < 0.05$ compared with acceptor cells with LV-control only. #Statistical significance $P < 0.05$ compared with acceptor cells with LV-*α-syn* alone. One-way ANOVA with *post hoc* Tukey–Krammer ($n = 3$ experiments per condition).

α-syn accumulation in DLB/PD and α-syn tg mice is associated with decreased CHMP2B protein

The co-culture system showed that the internalization and clearance of extracellular α-syn is dependent on the ESCRT pathway and previous studies have shown that alterations in the CHMP proteins might contribute to the neurodegenerative phenotype in FTD (14,15), ALS (16,17), AD (24), PD (25) and other neurodegenerative disease (19,20). To better understand the contribution of CHMPs to synucleinopathies *in vivo*, we examined fractionated brain lysates from DLB or control patients for protein levels of the ESCRT-III pathway. Interestingly, patients diagnosed with DLB showed reduced levels of cytosolic CHMP2B compared with control patients (Fig. 5A and B). Membrane-associated levels of CHMP3 and CHMP6 were also significantly reduced, whereas levels of CHMP4B/C were increased (Fig. 5C and D). We next isolated microvesicles from the whole brain homogenates from DLB and control patient brains to determine if α-syn was localized to these vesicles. Microvesicles isolated from DLB patient brains contained α-syn, whereas microvesicles isolated from control patients did not (Fig. 5E and F). These results were confirmed by immunocytochemistry showing reduced levels of CHMP2B, CHMP3 and CHMP6 with increased levels of staining for CHMP4B/C (Fig. 5G and H). Double immunolabeling and confocal imaging showed co-localization between large granular intraneuronal α-syn aggregates with CHMP2B and CHMP4B/C in the DLB cases but not in control cases (Fig. 5I and J). Consistent with these findings, analysis in mice of ESCRT-III proteins by immunoblot and immunocytochemistry showed reduced CHMP2B and CHMP3 and increased CHMP4 in α-syn tg mice with co-localization of CHMP2B with α-syn aggregates (Supplementary Material, Fig. S6). Further analysis of CHMP2B with the MVB protein (CD63) showed reduced co-localization in the DLB cases compared with control patients (Supplementary Material, Fig. S7A and B). Furthermore, combined immunogold and electron microscopy showed that compared with controls in the neuronal cells of the DLB cases, gold particles representing CHMP2B immunostaining were significantly reduced in association with the MVBs (Supplementary Material, Fig. S7C and D). In agreement with these results, compared with non-tg mice, the α-syn tg mice showed decreased CHMP2B/CD63 ratio (Supplementary Material, Fig. S7F and G), reduced CHMP2B gold in MVBs (Supplementary Material, Fig. S7H and I).

Taken together, these results suggest that alterations in the CHMPs in DLB and models of synucleinopathies might result in alterations in the trafficking and degradation of aggregated proteins such as α-syn. This also suggests that CHMP2B downregulation, similar to what was observed in the neuronal cells infected with LV-sh*CHMP2B* in the co-culture system, could also lead to alterations in the clearance of extracellular α-syn worsening the degenerative phenotype.

Given that among others, CHMP2B protein levels are decreased in DLB and models of synucleinopathies, we examined whether this decrease was due to decreased transcription of CHMP2B mRNA or increased degradation of CHMP2B protein. Real-time PCR analysis of CHMP2B mRNA in DLB patients (Supplementary Material, Fig. S7E) and in α-syn tg mice (Supplementary Material, Fig. S7J) indicated no significant difference in transcription of mRNA compared with controls. Given that α-syn co-localizes with CHMP2B in intracellular granular

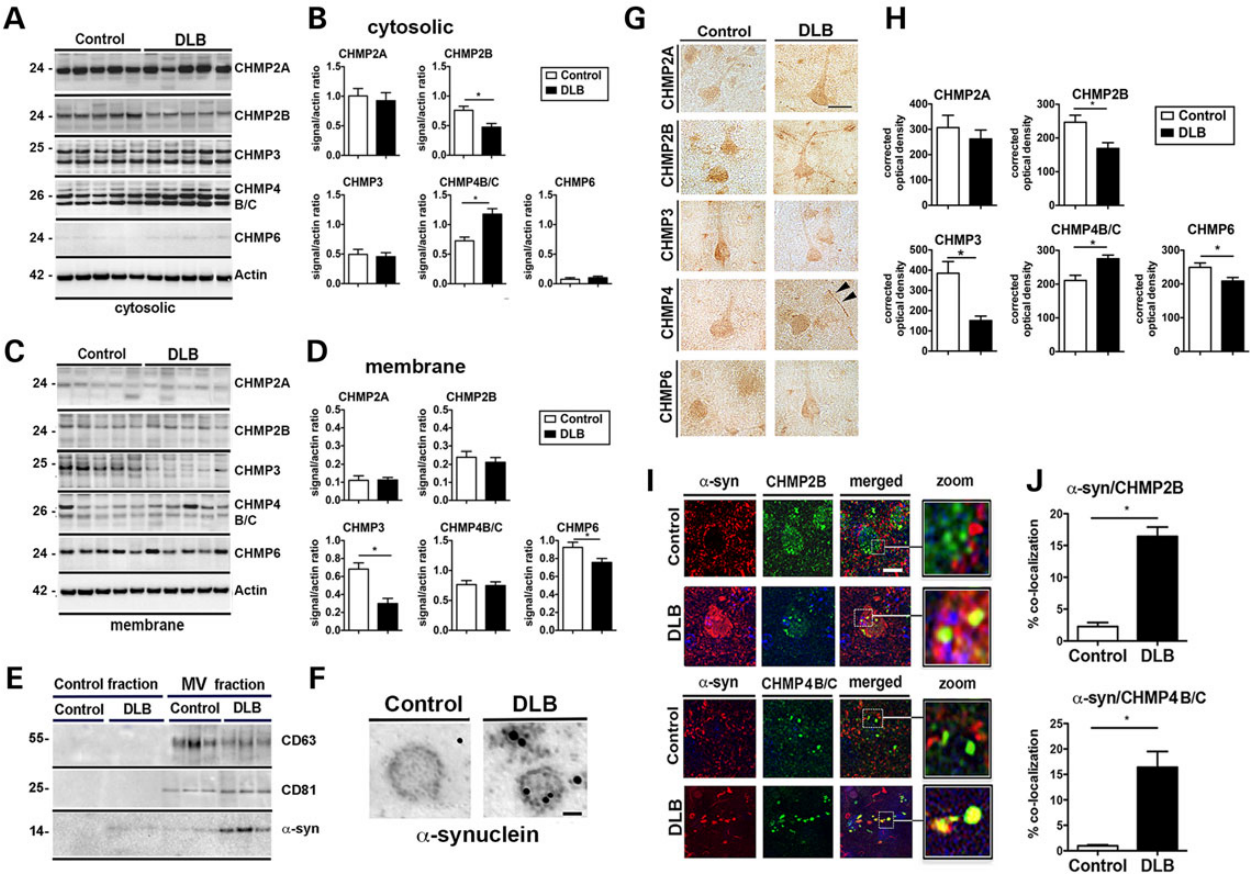

Figure 5. Dysregulation of ESCRT-III proteins in DLB. Western blot analysis of (**A**) cytosolic and (**C**) membrane fractions of brain homogenates showing levels of ESCRT-III complex proteins CHMP2A, CHMP2B, CHMP3, CHMP4B/C and CHMP6 on postmortem human brain samples from control subjects and DLB patients. Densitometric analysis of (**B**) cytosolic and (**D**) membrane fraction western blots of CHMP2A, CHMP2B, CHMP3, CHMP4B/C and CHMP6 immunoreactivity analyzed as ratio to β-actin signal. (**E**) Microvesicles (MV) isolated from whole brain homogenates of normal or DLB patient brains were analyzed by immunoblot for the multivesicular body marker CD63 and CD81 as well as the presence of α-syn. (**F**) Electron microscopy of isolated MV stained with gold particle labeled anti-α-syn. Scale bar = 50 nm ($n = 4$ control and $n = 4$ DLB cases). (**G**) Immunohistochemical detection of CHMP2A, CHMP2B, CHMP3 and CHMP4B/C in control and DLB brains. Scale bar = 20 µm. Arrowheads indicate Lewy neurite. (**H**) Optical density analysis of immunohistochemical immunoreactivity. (**I**) Brain sections from the control subject and DLB patients were double labeled with antibodies against α-syn (red) and CHMP2B or CHMP4B/C (green) and imaged with the laser scanning confocal microscope. (**J**) Analysis of % of cells showing co-localization between α-syn and CHMP2B or CHMP4B/C. *Indicates statistical significance $P < 0.05$ compared with control subjects. One-way ANOVA with *post hoc* Tukey–Krammer ($n = 8$ control cases and $n = 12$ DLB cases).

aggregates, we hypothesized that increased levels of intracellular α-syn might lead to increased degradation of CHMP2B. To determine the route of CHMP2B degradation, the neuronal cell line B103 was infected with the LV-*α-syn* vector to increase the intracellular accumulation of α-syn and then examined for endogenous CHMP2B in the presence of proteasome or autophagy modulators (Fig. 6). Overexpression of α-syn in the B103 cells reduced endogenous levels of CHMP2B (Fig. 6A–F) similar to the observation in human DLB patients (Fig. 5) and α-syn tg mice (Supplementary Material, Fig. S6). In cells overexpressing α-syn, treatment with BafA1, an autophagy inhibitor, blocked the degradation of CHMP2B, whereas treatment with lactacystin, a proteosome inhibitor, had much less effect on the levels of CHMP2B (not shown). This suggests that the α-syn-induced degradation of CHMP2B occurs primarily through the autophagy pathway. Similarly, treatment of cells with the autophagy inducer rapamycin increased the degradation of CHMP2B (Fig. 6A–F). In this system, compared with LV-control, levels of α-syn immunoreactivity were considerably elevated in the LV-*α-syn* group and were further elevated by treatments with BafA1 and lactacystin, whereas rapamycin decreased α-syn accumulation (Fig. 6A–F). Together, these results suggest that intracellular accumulation of α-syn might interact with CHMP2B inducing CHMP2B degradation; the reduced levels of CHMP2B might in turn result in defective internalization of extracellular aggregates such as α-syn further worsening of the degenerative phenotype (Fig. 6G).

Further analysis of α-syn and CHMP2B potential interaction was performed by co-immunoprecipitation with the brains of α-syn tg and DLB patients with an antibody against CHMP2B and then probed for α-syn. We observed α-syn interaction with CHMP2B in α-syn tg mice and in DLB patient brains but not in non-tg mouse or control human brains (Supplementary Material, Fig. S8A). This was confirmed by co-immunolocalization with antibodies for α-syn and CHMP2B in sections from α-syn tg and DLB human brains where CHMP2B immunoreactive granular structures were co-localized with α-syn immunoreactive Lewy body-like intraneuronal inclusions (Supplementary Material, Fig. S8B).

Increasing CHMP2B *in vivo* can reduce *α-syn* accumulation and ameliorate the neurodegenerative pathology in transgenic mice

Because CHMP2B is downregulated in mouse models and patients with DLB, then it is possible that increasing the expression

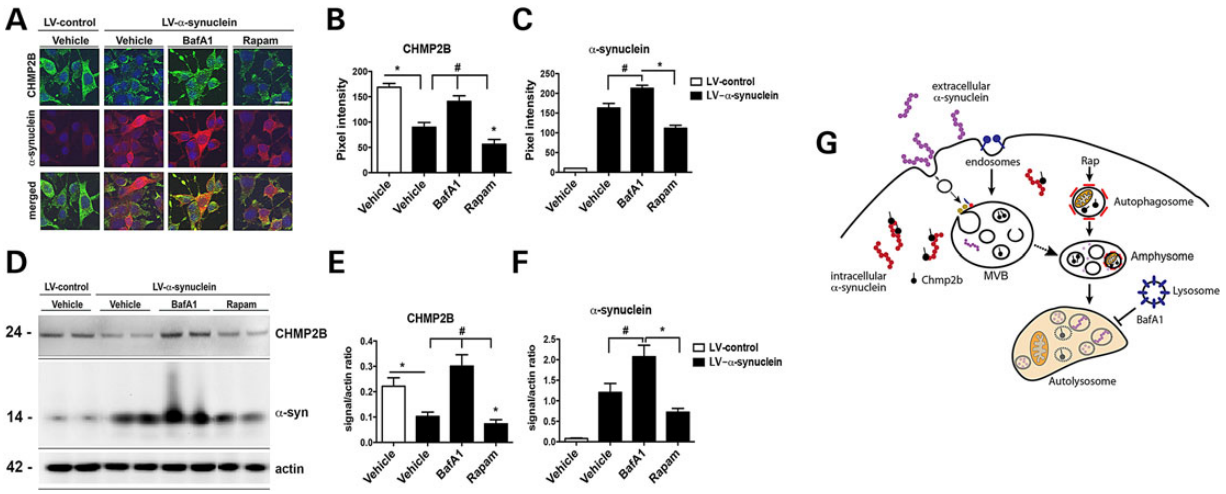

Figure 6. α-syn overexpression leads to CHMP2B degradation through the autophagy pathway. B103 neuronal cells were infected with LV-*α-syn* or LV-control and then treated with BafA1, Rapamycin (Rapam) or vehicle (control). (**A**) Immunohistochemistry of fixed cells with α-syn (red), CHMP2B (green) and nuclei (DAPI, blue). Optical density analysis of immunohistochemical immunoreactivity for (**B**) CHMP2B and (**C**) α-syn is calculated as pixel intensity. (**D**) Representative immunoblot of B103 cells infected with LV-control of LV-*α-syn* and treated with BafA1, Rapam or Vehicle. Quantitative densitometry of immunoblot for (**E**) CHMP2B and (**F**) α-syn normalized to actin signal. (**G**) Model of intracellular α-syn affecting CHMP2B degradation and its effects on endocytosis of extracellular α-syn. *Indicates statistical significance $P < 0.05$ compared with LV-control-infected cells. #Statistical significance $P < 0.05$ compared with vehicle treated LV-α-syn-infected cells. One-way ANOVA with *post hoc* Tukey–Krammer ($n = 3$ wells for each experiment).

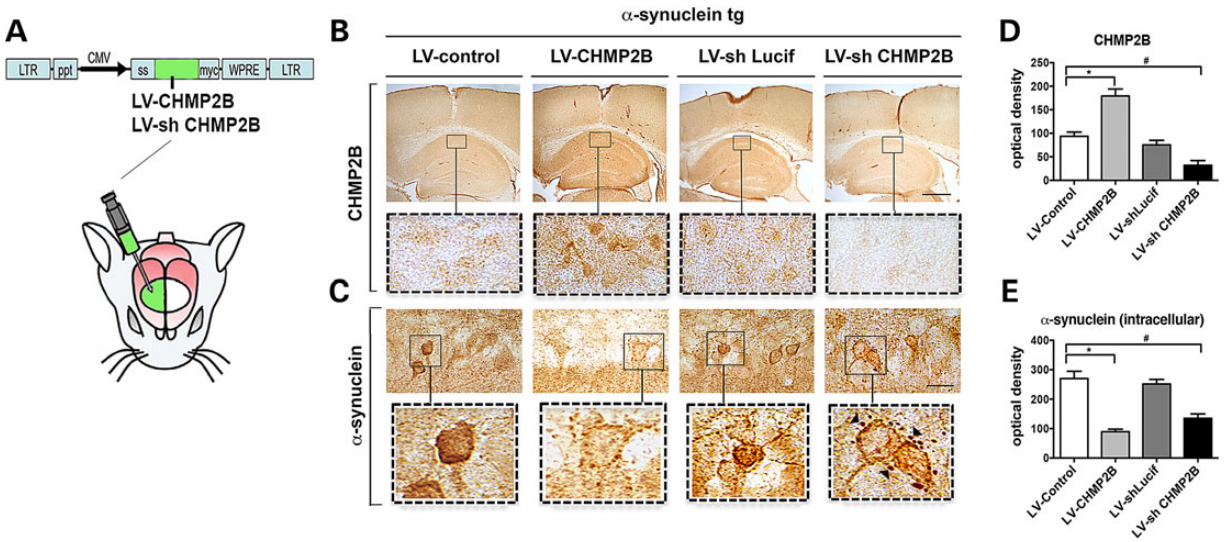

Figure 7. Lentivirus overexpression of CHMP2B reduces accumulation of α-syn in the α-syn tg mouse model of DLB. (**A**) The LV-*CHMP2B*, LV-Control, LV-sh*CHMP2B* or LV-sh*Lucif* lentivirus vectors were delivered by stereotaxic injection into the hippocampus of α-syn tg mouse model of DLB. (**B** and **D**) Four weeks after injection, mice were sacrificed and brains were analyzed by immunohistochemistry and computer-aided image analysis for CHMP2B. (**C** and **E**) Brains were analyzed by immunohistochemistry for α-syn. Arrowheads indicate pericellular α-syn aggregates. *Indicates statistical significance $P < 0.05$ compared with treatment with LV-control. One-way ANOVA with *post hoc* Tukey–Krammer. Scale bar represents 200 µm in low power images and 40 µm in high power images ($n = 10$ mice per group).

of CHMP2B could overcome this blockade and reduce the accumulation of internalized α-syn as we showed in the *in vitro* experiments (Fig. 2). To investigate this possibility *in vivo*, the LV-*CHMP2B* or LV-sh*CHMP2B* vectors were injected into the hippocampus of non-tg and α-syn tg model of DLB (Fig. 7A). Intracerebral delivery of LV-*CHMP2B* significantly increased expression of CHMP2B throughout the hippocampus in neuronal soma, whereas the sh*CHMP2B* decreased the expression of this protein in pyramidal cells in the hippocampus (Fig. 7B and D). In this tg model of DLB, α-syn accumulates in neuritic processes, synapses and neuronal cell bodies in the CA1 and CA3 regions. Compared with mice injected with LV-control, the α-syn tg mice that received LV-*CHMP2B* showed a significant reduction in the accumulation of α-syn in the neuronal cell bodies and neurites in the hippocampus (Fig. 7C and E). Compared with mice that received LV-sh*Lucif* (as control), α-syn tg mice that were injected with LV-sh*CHMP2B* displayed reduced intraneuronal α-syn; however, there was a considerable increase and re-localization of α-syn immunoreactivity to the surface of the neurons and to granular structures in the perineuronal region (Fig. 7C and E) similar to the results obtained for the *in vitro* experiments (Fig. 2E).

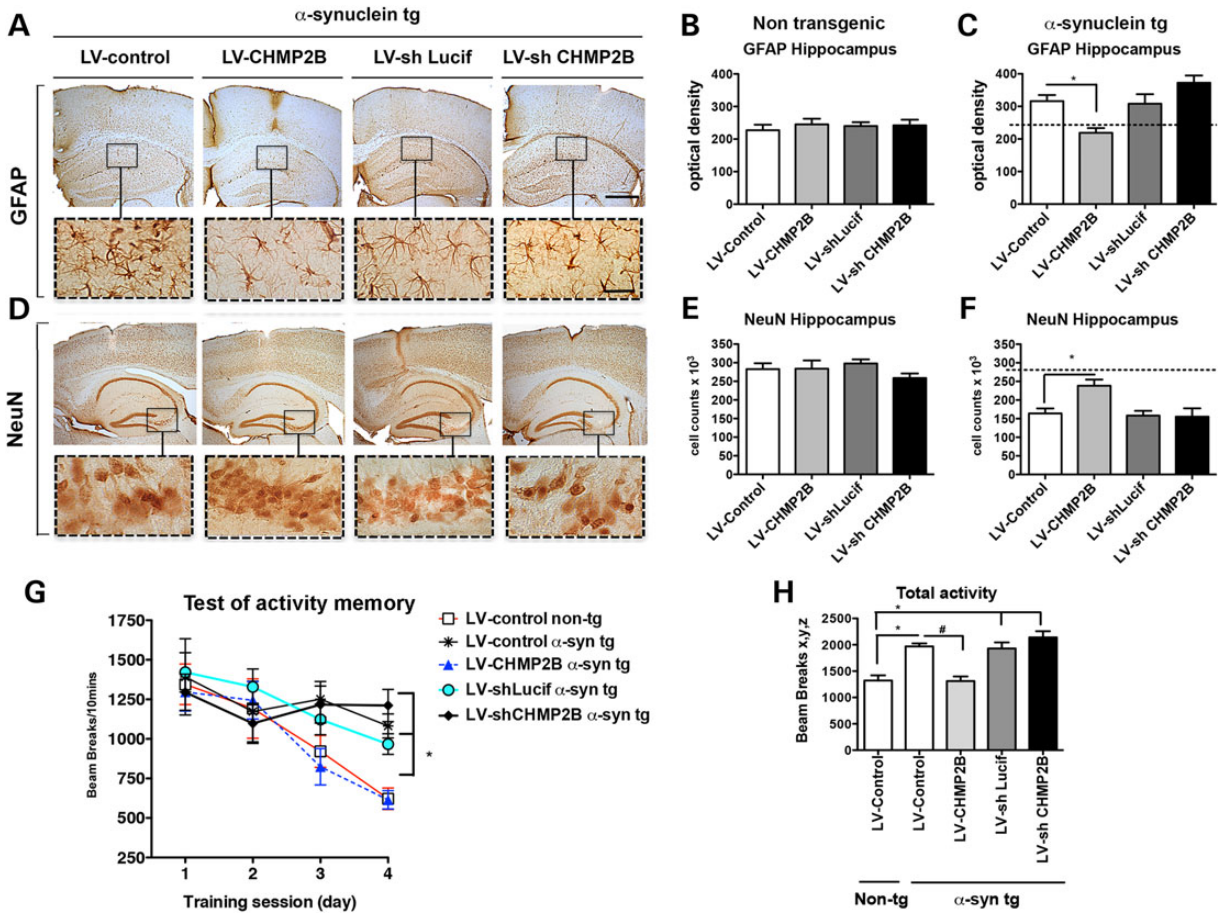

Figure 8. Lentivirus overexpression of CHMP2B ameliorates neurodegeneration and behavior deficits in the α-syn tg mouse model of DLB. The LV-*CHMP2B*, LV-control, LV-sh*CHMP2B* or LV-sh*Lucif* lentivirus vectors were delivered by stereotaxic injection to the D-line α-syn tg mouse model of DLB. Four weeks after injection, mice were sacrificed and brains were analyzed by immunohistochemistry for (**A**) GFAP and (**D**) NeuN. Insets show high power magnification of sections from the hippocampus. Optical density analysis of immunohistochemical immunoreactivity of GFAP in the hippocampus was analyzed in (**B**) non-tg and (**C**) α-syn tg mice. Stereological estimates (dissector method) of total NeuN positive neuronal counts was measured in the hippocampus of (**E**) non-tg and (**F**) α-syn tg mice. (**G**) Behavioral performance analysis in the context-dependent learning in an open field test. (**H**) Total activity on Day 4 in the open field. *Indicates statistical significance $P < 0.05$ compared with treatment with LV-control non-tg. #Statistical significance $P < 0.05$ compared with LV-control α-syn tg. One-way ANOVA with *post hoc* Tukey–Krammer. Scale bar represents 200 μm in low power images and 40 μm in high power images ($n = 10$ non-tg and tg mice per group).

We have previously reported that the α-syn tg model displays astrogliosis and loss of neurons in the CA3 region of the hippocampus (26,27). To evaluate the effects on neurodegeneration of modulating CHMP2B in the α-syn tg mouse, levels of GFAP and NeuN were analyzed. Compared with non-tg mice, α-syn tg mice treated with the LV-control displayed increased GFAP immunoreactivity (Fig. 8A–C) and decreased NeuN neurons in CA3 (Fig. 8D–F). Treatment of α-syn tg mice with the LV-*CHMP2B* restored levels of GFAP immunoreactivity (Fig. 8A–C) and NeuN cell counts in CA3 comparable to non-tg controls (Fig. 8D–F). In contrast, α-syn tg mice treated with the LV-sh*CHMP2B* displayed significant astrogliosis and neuronal loss (Fig. 8C and F).

In our DLB-like tg model, the abnormal accumulation of α-syn in the limbic system is associated with memory deficits (28). For this reason to evaluate the effects of CHMP2B in the α-syn tg mice, the context-dependent learning in an open field test was performed. Compared with the LV-control injected non-tg mice, the LV-sh*Lucif* α-syn tg displayed increased activity and reduced habituation to the novel environment indicating learning deficits (Fig. 8G). In contrast, α-syn tg mice that received LV-*CHMP2B* performed similar to the LV-control non-tg, whereas mice that received the LV-sh*CHMP2B* performed slightly worse than the α-syn tg mice injected with the LV-sh*Lucif* (Fig. 8G). Compared with α-syn tg mice on Day 4, mice treated with LV-*CHMP2B* showed significantly less hyperactivity and were similar to LV-control-treated non-tg mice (Fig. 8H). These studies suggest that upregulating CHMP2B via gene therapy with lentiviral vectors reduces the intracellular accumulation of α-syn and ameliorates the neurodegenerative and behavioral alterations in a tg model of DLB.

Discussion

In this study, we showed that once endocytosed, extracellular α-syn is transported to the autophagosome for degradation through the ESCRT system in MVBs. This transport mechanism might be disrupted by reduced levels of CHMP2B thus generating a roadblock for the internalization of α-syn resulting in abnormal accumulation in the pericellular region and impaired lysosomal degradation. This could lead to neuronal dysfunction in the newly 'infected' neuron, which propagates the α-syn pathology. Moreover, in the brains of DLB patients as well as in models of synucleinopathies, CHMP2B is reduced. Gene therapy with LV-

CHMP2B reduces the neuronal accumulation of α-syn and ameliorates the neurodegenerative pathology in tg mice.

Propagation of α-syn from neuron-to-neuron and neuron-to-glial cells has been proposed to play an important role in the mechanisms of neurodegeneration and progression of the functional deficits in PD/DLB patients (8,29,30). The transfer of α-syn from cell-to-cell requires several independent steps including (1) secretion from donor cells, (2) receptor binding to acceptor cells, (3) internalization/endocytosis by acceptor cells and (4) intracellular trafficking in acceptor cells (31). The characteristics of the secreted α-syn in this study are in agreement with our previous studies showing that in this system there is both monomeric and multimeric forms of α-syn present in donor cells and conditioned media (21). The question of secretion of α-syn aggregates by donor cells has been extensively investigated and appears to involve a tetradotoxin-dependent clear vesicle pathway, exosome-mediated release (32–34) and membrane penetration (35–37). Overexpression of CHMP2B in the α-syn tg model of DLB appeared to reduce the neuronal accumulation of α-syn and improve memory deficits measured in the mice. We have previously shown α-syn accumulation in astrocytes and microglia in these animals; however, because the lentivirus vector used to deliver the CHMP2B gene primarily infects neurons, we focused our analysis on neuronal α-syn accumulation.

Previous studies have shown, and we confirm in this study, that α-syn is endocytosed by acceptor cells via a dynamin-dependent pathway (34) wherein some instances it could traffic into the endosomal/lysosomal pathway for degradation (38,39). However, less is known about the mechanisms of cellular trafficking and alterations in PD/DLB. This study bridges this gap by providing new evidence showing that ESCRT-III-dependent formation of MVBs plays a key role by transporting the α-syn from the endosome to the autophagy pathway. The ESCRT-III set of proteins of the ESCRT family targets vesicles for the formation of MVBs through its unique ability to perform membrane remodeling by inducing cell invagination away from cell cytoplasm. This allows the formation of large MVBs that act as a depot for proteins and organelles in transit for autophagy-mediated degradation. The process of invagination of the endosome into the MVB begins with the binding of CHMP4 and CHMP6 to the membrane. This complex recruits CHMP3 and either CHMP2A or CHMP2B (40). Previous studies have shown that CHMP2A and CHMP2B differentially interact with distinct endosomal vesicles for trafficking to the MVB (41). In fact, in our study, we observed reduced trafficking of α-syn when CHMP2B was reduced by short-hairpin RNA (shRNA) but not when CHMP2A was reduced by siRNA. Thus, it would appear that α-syn-containing endosomes are targeted to the MVB by CHMP2B specifically.

CHMP2B is a 24 kDa protein that is part of the ESCRT-III complex that plays a role in the transport of proteins from endosomes to lysosomes (42). This process is dependent on the interactions between the C-terminus of CHMP2B with the ATPase of VPS4 (43). VPS34 is also responsible for the final disassembly of the full ESCRT-III complex after membrane scission (43). Because CHMP2B is recruited only after CHMP4 is already localized at the membrane, it may be that downregulation or reduced CHMP2B levels leave CHMP4 protein bound to the membrane thus stabilizing levels of CHMP4 protein. This may account for the increased levels of CHMP4 we observed in both DLB patients and α-syn tg mice when CHMP2B and CHMP3 are reduced.

Under physiological conditions, this CHMP2B-mediated process might allow the clearance of aggregated proteins such as α-syn via autophagy; however, we propose that in PD/DLB this process is disrupted. In our model, we present evidence supporting the possibility that the intracellular aggregates of α-syn can interact with CHMP2B resulting in targeted degradation of this ESCRT-III. Reduced CHMP2B blocks the transit of newly formed endocytic vesicles containing α-syn from being targeted to the autophagosome for degradation resulting in an accumulation of these aggregates at the pericellular membrane or possibly recycling of endocytic vesicles to the extracellular space ultimately leading to neurotoxicity. The characteristics and mechanisms through which intracellular α-syn binds and disrupts ESCRT-III is unclear; however, a recent report suggested that endocytosed α-syn aggregates targeted to lysosomes could rupture the lysosome membrane leading to entry to the cytoplasm (44) where it could potentially interact with components of the ESCRT-III pathway. Thus, the propagated α-syn could be the source of the intracellular interference that leads to an accumulation of α-syn at the pericellular membrane, thus forming a feedback loop. However, additional studies need to be completed in order to confirm these findings.

In fact, the question of how the spread of α-syn from cell-to-cell can occur if intracellular α-syn is interfering with the uptake of this extracellular α-syn has not escaped our attention. Extracellular α-syn presumably is initially released from affected cells in brain regions such as the brainstem, caudate or olfactory bulb where areas of α-syn accumulation are first observed (45–47). This extracellular α-syn would encounter cells with low levels of endogenous α-syn with an intact ESCRT system leading to MVB formation and autophagy-mediated degradation. Some of this endocytosed α-syn could leak from the endolysosome of the newly 'infected' neuron and interact with the endogenous α-syn seeding aggregation (44). These intracellular aggregates would lead to decreased CHMP2B protein levels, decreased ESCRT-III function and decreased internalization/degradation of the extracellular α-syn. We showed that downregulation of CHMP2B in cells in culture led to an increase in cell-to-cell spread and uptake of α-syn form those same cells. Therefore, the increased uptake of α-syn, leading to the targeted degradation of CHMP2B leads to increased cell-to-cell propagation of α-syn providing a positive feedback loop perpetuating the disease synucleinopathy. It should also be noted that while these experiments were designed to investigate the effects of CHMP2B on the endocytosis and exocytosis of α-syn, there might be many other proteins affected by the dysregulation of the ESCRT system.

A model for α-syn interfering with its own clearance is in agreement with previous studies that have shown that autophagy is altered in PD/DLB (48,49). For example, α-syn mutations associated with familial PD and post-translational modifications such as oxidation have been shown to interfere with chaperone-mediated autophagy (49). Moreover, we have found that in DLB and in α-syn tg models, mTor and ATG7 are dysregulated resulting in reduced autophagy (22,23). Additionally, defective autophagy results in increased release of α-syn (50). In this study, we propose that, α-syn either aggregating intracellularly or endocytosed α-syn aggregates leaking from the endosome/lysosome could bind to CHMP2B disrupting the ESCRT pathway. Studies in yeast reveal that depletion of any component of the ESCRT-III complex can completely block the formation of MVB (11). For this study, we found that several components of the ESCRT-III system such as CHMP2B, CHMP3 and CHMP4 are altered in DLB and that CHMP2B is co-localized with intracellular α-syn aggregates and with Lewy bodies in DLB and α-syn tg mice. This is consistent with previous studies that have shown that CHMP2B immunoreactivity is present in LB's in PD (25) and other synucleinopathies (51), and we show here that CHMP2B and α-syn co-precipitate in DLB and tg mice.

Table 1. Summary of human cases

Group	N	Mean age (yrs)	Gender M/F	PMT (h)	Braak stage	Blessed score	Brain weight (gms)	LB's in neocortex (score)	LB's in midbrain (score)
Control	8	76 ± 10	3/5	8 ± 13	0	0	1215 ± 90	0	0
DLB	12	83 ± 5	6/6	9 ± 1.5	III–IV	26 ± 2	1110 ± 95	3+	2+

PMT, postmortem time.

Interestingly, CHMP2B mutations have been shown to be a rare cause of autosomal dominant FTD linked to chromosome 3 (FTD-3) which was described in a Danish cohort, with a further CHMP2B mutation identified in an unrelated patient with FTD in Belgium (14,52–54). These mutations result in C-terminal truncations of the CHMP2B protein that results in alterations in vesicular fusion events within the endosome–lysosome and autophagy degradation pathways (52). The mutation occurs in the splice acceptor site for the sixth and final *CHMP2B* exon, leading to the formation of two novel transcripts termed *CHMP2BIntron5* and *CHMP2BDelta10*. Missense mutations in CHMP2B have also been associated with the FTD-motor neuron disease spectrum of disorders (52).

Overexpression of mutant CHMP2B in tg mice has been described to mimic some aspects of FTD including decreased survival and gliosis and accumulation of p62- and ubiquitin-positive inclusions (55). These findings were not observed in CHMP2B knockout mice or in transgenic mice expressing wild-type CHMP2B, suggesting that CHMP2B mutations promote neuropathology via gain of function (56). Similarly, although lentivirus delivery of shRNA-directed against CHMP2B was able to knockdown the expression of the protein in α-syn tg mice; we did not observed a significant increase in α-syn accumulation or any increase in neuropathology. Interestingly, we found that gene therapy with LV-*CHMP2B* rescued the alterations in the ESCRT-III pathway, enhanced autophagy, reduced accumulation of α-syn and ameliorated the neurodegenerative pathology in cellular and animal models. This suggests that at least in models of DLB where endogenous expression of CHMP2B is normal and increased accumulation of α-syn is pathogenic, overexpression of CHMP2B might rescue the pathology. In contrast, in models of FTD-3 where mutant CHMP2B is present, downregulation of the dominant mutant protein expression may be required to observe an effect (57).

In conclusion, we report that propagating extracellular α-syn is endocytosed by the ESCRT pathway and targeted for degradation by autophagy through the MVBs. Remarkably, in patients with DLB and in α-syn tg mice, levels of CHMP2B (and CHMP3) were reduced resulting in impaired degradation and trafficking of endocytosed extracellular α-syn. Delivery via gene therapy of CHMP2B ameliorated this block. This study supports a role of alterations of CHMP2B in the prion-like propagation and impaired clearance of α-syn and suggests that increasing CHMP2B might be of therapeutic value.

Materials and Methods

Animal care

All experiments described were carried out in strict accordance with good animal practice according to NIH recommendations, and all procedures for animal use were approved by the Institutional Animal Care and Use Committee at the University of California at San Diego (UCSD) under protocol #S02221.

Human specimens, neuropathological evaluation and criteria for diagnosis

A total of 20 cases ($n = 8$ non-demented controls and $n = 12$ DLB cases) were included for this study. Autopsy material was obtained from patients (Table 1) studied neurologically and psychometrically at the Alzheimer Disease Research Center/ University of California, San Diego (ADRC/UCSD). The last neurobehavioral evaluation was performed within 12 months before death and included Blessed score, Mini Mental State Examination and dementia-rating scale (58,59). Brains were processed and evaluated according to standard methods (60). At autopsy, brains were divided sagitally; the left hemibrain was fixed in formalin of 4% paraformaldehyde (PFA) for neuropathological analysis and the right frozen at −70°C for subsequent neurochemical analysis. Paraffin sections from 10% buffered formalin-fixed neocortical, limbic system and subcortical material stained with hematoxylin and eosin, thioflavin S, ubiquitin (Dako, Z0458) and α-syn (Millipore, AB5038P) were used for routine neuropathological analysis that included assessment of plaques, tangles, Lewy bodies and Braak stage (60). The diagnosis of DLB was based in the initial clinical presentation with dementia followed by parkinsonism and the presence of α-syn and ubiquitin-positive LBs in cortical and subcortical regions (61,62).

Construction of lentivirus vectors

The Flag-tagged mouse Chmp2B was a generous gift from Fen-Biao Gao (63). The Chmp2B cDNA was PCR amplified and cloned into the LV to generate LV-Chmp2B. An shRNA designed against the mouse Chmp2B (aa575-596) was cloned into the pSuper-GFP vector as previously described (63) to generate LV-shChmp2B. The control shRNA lentivector (LV-shLucif) contains an shRNA-directed against firefly luciferase.

The lentivirus vector expressing the human wild-type α-syn and myc-tagged α-syn have been previously described (64,65). Lentiviruses were prepared by transient transfection in 293T cells (66).

Establishment of a neuronal cell line expressing α-syn and ESCRT-III proteins

For these experiments, we used the rat neuroblastoma cell line B103. This model was selected, because overexpression of α-syn in these cells results in mitochondrial alterations, reduced cell viability, defective neurite outgrowth and abnormal accumulation of oligomeric α-syn (67). For all experiments, cells were infected with LV expressing wt α-syn at a multiplicity of infection (MOI) of 20.

The neuronal cell line was grown as described above and plated onto poly-l-lysine-coated glass coverslips at a density of 5×10^4 cells. Five hours after plating, cells were infected with the LV-α-syn at an MOI of 20 and incubated for 48 h. Control experiments were performed with cells infected with LV-control. Cell viability was assayed by LDH release (CytoTox NonRadioactive Cytotoxicity Assay, Promega) (22).

For siRNA transfection experiments, B103 cells were plated at a density of 5×10^4 cells per well of a 12-well dish and transfected with siPort NeoFX reagent (Ambion) according to manufacturer's directions. Five nanomolar of siCHMP2A (ID#26027, Ambion), siCHMP6 (ID#35989, Ambion) or siCtrl (Ambion) were added to each well in Optimem. Cells were incubated for 6 h and then refed complete media. Forty-eight hours after transfection, cells were co-cultured with inserts containing B103 cells infected with LV-control or LV-*α-syn* for 24 h prior to fixation with 4% PFA.

For co-culture analysis, 5×10^4 B103 cells were plated onto poly-l-lysine-coated glass coverslips or onto 12-well cell culture inserts containing a 0.4 µm PET membrane (Fisher Scientific). Cultures were incubated separately for 6 h to allow cells to attach and then co-cultured until analysis. To examine the effects on the autophagy pathway, lactacystin (2.5 µm—24 h, Sigma), rapamycin (200 nm—6 h or 10 nM—24 h, Sigma) or BafA1 (200 nM—6 h, Sigma) was added prior to fixation (22). For serum starvation, B103 cells were washed twice with warm PBS and then incubated in DMEM with 0.5% FBS for 18 h to induce autophagy. Additionally, experiments were conducted with Dynasore, a dynamin GTPase inhibitor (68). B103 cells infected with LV-control or LV-*α-syn* were plated at 5×10^4 cells per well of 12-well dish on poly-lysine-coated glass coverslips for 24 h. Cells were treated with 80 µm Dynasore dissolved in DMSO or control DMSO for 30 min at 37°C. Cells then were treated with oligomerized human α-syn for 10 min at 37°C.

Primary mouse cortical neurons (Life Technologies) were plated on poly-lysine-coated glass coverslips in 12-well dishes and grown according to manufacturer's directions. Ten days after plating, cells were infected with LV-control, LV-*CHMP2B* or LV-sh*CHMP2B* at MOI = 50. Forty-eight hours after infection, mouse cortical cells were co-cultured with B103 cells previously infected with LV-control or LV-*α-syn* for 48 h.

At the conclusion of all experiments, cells were washed twice with ice-cold PBS followed by fixation with cold 4% PFA.

Real-time PCR analysis

Total RNA was isolated from mice brains using the RNeasy lipid mini kit (Qiagen) and was reverse transcribed using RT^2 First Strand kit (Qiagen) from 1 µg of total RNA. Real-time PCR analysis was performed using the StepOnePlus real-time PCR system (Applied Biosystems) with primers specific for human or mouse CHMP2B (Life Technologies). Relative quantification of gene expression was calculated by the comparative threshold cycle (Ct) method and expressed as 2-exp (ΔΔCt) using mouse β-actin as an internal control as previously described (69).

α-syn quantitative assay

Following co-culture with α-syn-expressing cells, culture supernatant was assayed with the Human α-syn Electroluminescence Assay (MesoScale Discovery) at a 1:2 dilution according to manufacturer's directions. α-syn quantities were determined with a standard curve of recombinant human α-syn.

Microvesicle isolation

Isolation of microvesicles from frozen tissue was performed as previously described (70). Frozen frontal cortex (2 g) was dissected and treated with 20 units/ml of papain in Hibernate E (Life Technologies) (10:1 ration) for 15 min at 37°C. Then, 20 ml of cold Hibernate E is added, and the solution is gently homogenated. The brain homogenate is filtered through a 40 µl mesh filter, and the supernatant is serial centrifugation: 300*g* for 10 min, 2000*g* for 10 min, 10 000*g* for 30 min. The supernatant is then passed through a 0.2 µm filter. And centrifuged at 100 000*g* for 70 min at 4°C. The pellet contains the microvesicle fraction. This fraction is then further cleaned by washing twice in PBS followed by centrifugation at 100 000*g* for 80 min. The purity of microvesicles is confirmed by the presence of CD63 (Systems Bioscience, EXOAB-CD63A-1) and CD81 (Systems Bioscience, EXOAB-CD81A-1) through immunoblot.

Co-immunoprecipitation of CHMP2B

All procedures for immunoprecipitation were performed at 4°C. Human and mice brains were lysed using PDGF buffer (1 mm HEPES, 5 mm benzamidine, 2 mm 2-mercaptoethanol, 3 mm EDTA, 0.5 mm $MgSO_4$ and 0.05% NaN_3) with phosphatase and protease inhibitor cocktails (Roche Applied Science). After a brief sonication, samples were centrifuged for 5 min at 5000*g*. Dynabeads Protein A (Life Technologies) were pre-incubated with 5 µg of normal rabbit IgG or anti-CHMP2B (Abcam, ab76332) for 1 h, and then beads were washed with ice-cold PBS for three times. A total of 10 mg of each brain homogenate was then added to the antibody-Dynabeads. After overnight incubation, samples were washed (0.1% Triton X-100, 150 mm NaCl in PBS) three times. Samples were resuspended in 1× sample buffer (Life Technologies) boiled 10 min and then analyzed by immunoblot.

Immunoblot analysis

Tissues were homogenized in TNE buffer (50 mm Tris–HCl, pH 7.4, 150 mm NaCl, 1 mm EDTA; all from Sigma-Aldrich) containing 1% Nonidet P-40 (Calbiochem) with protease and phosphatase inhibitor cocktails (Roche). Tissue homogenates were separated into cytosolic (soluble) and membrane (pellet) fractions by centrifugation at 100 000*g* for 1 h at 4°C (23). Protein concentration was assayed by BCA (Pierce Biotechnology, Rockford, IL, USA). For western blot analysis, 20 µg of each fraction was resolved on a 4–12% Bis–Tris SDS-PAGE gel and blotted onto polyvinylidene fluoride membranes. In addition, for tissue culture material neuronal cell lysates and conditioned media was concentrated and run on SDS-PAGE and native gels. Blots were incubated with antibodies against α-syn (Millipore, AB5038P, BD Biosciences, 610787, 5G4 clone Millipore mabn389), CHMP2A (Abcam, ab76335), CHMP2B (Abcam, ab76332), CHMP3 (Abcam, ab76333), CHMP4B/C (recognizes both CHMP4B and CHMP4C) (Abcam, ab76334), CHMP6 (Abcam, ab67168), CD63 (Systems Bioscience), CD81 (Systems Bioscience) and actin (Millipore, mab1501) followed by secondary antibodies tagged with horseradish peroxidase (Santa Cruz), visualized by enhanced chemiluminescence and analyzed with a Versadoc XL imaging apparatus (BioRad). Analysis of actin levels was used as a loading control.

Transgenic mouse lines and injections of lentiviral vectors

For this study, mice overexpressing α-syn from the murine Thy1 promoter (line 61) (6 month old, male, C57/Bl6) were utilized (71). This model was selected, because mice from this line develop intraneuronal α-syn aggregates distributed through the brain similar to PD and DLB (72). A cohort of $n = 10$ non-tg and 40 tg (LV-control, LV-*CHMP2B*, LV-sh*Lucif*, LV-sh*CHMP2B*, $n = 10$ mice per group) was injected bilaterally with 3 µl each of the lentiviral preparations (2.5×10^7 TU) into the hippocampus (using a 5 µl Hamilton syringe) as previously described (73). We and others have previously shown that a single injection to the hippocampus in this region will generate transgene delivery throughout the whole hippocampus for up to 6 months after vector delivery (73–75). Mice survived for 4 weeks months after the lentiviral

injection. Brains and peripheral tissues were removed and divided sagitally. The right hemibrain was postfixed in phosphate-buffered 4% PFA (pH 7.4) at 4°C for 48 h for neuropathological analysis, whereas the left hemibrain was snap-frozen and stored at −70°C for subsequent protein analysis.

Behavioral analysis

Context-dependent learning in an open field was analyzed using a Kinder SmartFrame Cage Rack Station activity monitor system (Kinder Scientific, Poway, CA, USA), in three-dimensional space using a 7 × 15 beam configuration. Data collection began when an animal was placed in the test chamber. Animals were evaluated for 10 min for three consecutive days, given a 2-day dishabituation period, followed by a fourth trial (28,76).

Immunocytochemical and neuropathological analyses

Analysis of α-syn accumulation was performed in serially sectioned, free-floating, blind-coded vibratome sections from α-syn tg and non-tg (77). Sections were incubated overnight at 4°C with an anti-α-syn antibody (affinity purified rabbit polyclonal, Millipore) (78), followed by biotinylated goat anti-rabbit IgG (Vector Laboratories, Inc.), Avidin D-HRP (ABC Elite, Vector) and detection with the Tyramide Signal Amplification™-Direct (Red) system (NEN Life Sciences) to determine the number of α-syn immunoreactive inclusions in the neocortex. For each case, three sections were analyzed by the dissector method using the Stereo-Investigator System (MBF Bioscience), and the results were averaged and expressed as numbers per mm^3.

To determine the co-localization between α-syn immunolabeled-neurons and Chmp2B, 40 µm-thick vibratome sections were immunolabeled with the rabbit polyclonal antibody against α-syn (Millipore) (78) and the Chmp2B (Abcam) antibody. The α-syn immunoreactive structures were detected with the Tyramide Signal Amplification™-Direct (Red) system (NEN Life Sciences), whereas the Chmp2B was detected with the horse anti-mouse IgG fluorescein isothiocyanate (FITC) antibody (Vector).

To determine if the CHMP2B gene transfer ameliorated, the neurodegenerative alterations associated with the expression of α-syn, briefly as previously described (79,80), blind-coded, 40-µm-thick vibratome sections from mouse brains fixed in 4% PFA were immunolabeled with the mouse monoclonal antibodies against NeuN (neuronal marker, Millipore, mab377) or glial fibrillary acidic protein (GFAP, astroglial marker, Millipore, mab3402) (81). After overnight incubation with the primary antibodies, sections were incubated with biotinylated secondary antibody and reacted with diaminobenzidine. All sections were processed under the same standardized conditions. The immunolabeled blind-coded sections were serially imaged with the LSCM and analyzed with the Image 1.43 program (NIH), as previously described (81,82). For each mouse, a total of three sections from the hippocampus and three from the cortex were analyzed and for each section, four fields in the frontal cortex and hippocampus were examined. All sections were processed simultaneously under the same conditions and experiments were performed twice in order to assess the reproducibility of results. Sections were imaged with a Zeiss 63× (N.A. 1.4) objective on an Axiovert 35 microscope (Zeiss) with an attached MRC1024 LSCM system (BioRad) (78).

Double immunolabeling and fluorescence co-labeling

To determine the co-localization between α-syn, ESCRT and autophagy markers double-labeling experiments were performed, as previously described (83). For this purpose, vibratome sections were immunolabeled with the antibodies against α-syn (BD Biosciences or Millipore, MABN389, 5G4 clone Millipore mabn389), c-myc (9E10, Sigma, m5546) CHMP2A (Abcam), CHMP2B (Abcam), CHMP4B/C (Abcam), CD63 (System Biosciences), LC3 (Abcam, ab4753) or LAMP2 (Santa Cruz, sc8100). The α-syn, immunoreactive structures were detected with the Tyramide Signal Amplification™-Direct (Red) system (NEN Life Sciences), whereas the other antibodies were detected with FITC-tagged secondary antibodies (Vector). All sections were processed simultaneously under the same conditions, and experiments were performed twice in order to assess the reproducibility of results. Sections were imaged with a Zeiss 63× (N.A. 1.4) objective on an Axiovert 35 microscope (Zeiss) with an attached MRC1024 LSCM system (BioRad) (78).

Electron microscopy and immunogold analysis

Briefly, vibratome sections were postfixed in 1% glutaraldehyde, then treated with osmium tetraoxide, embedded in epon araldite and sectioned with the ultramicrotome (Leica). Grids were analyzed with a Zeiss OM 10 electron microscope as previously described (84). For immunogold labeling, sections were mounted in nickel grids, etched and incubated with antibodies against α-syn (Millipore, MABN389) or Chmp2B (Abcam) followed by labeling with 10 nm Aurion ImmunoGold particles (Electron Microscopy Sciences) with silver enhancement. A total of 125 cells were analyzed per condition. Cells were randomly acquired from three grids, and electron micrographs were obtained at a magnification of 25 000×.

Intracellular localization analysis

Briefly, as previously described, coverslips double labeled with antibodies against the neuronal marker MAP2 (Millipore, mab3418) (FITC) and α-syn (Life Technologies, 328100) (Tyramide Red) were mounted on superfrost slides (Fisher) containing DAPI and imaged with a Zeiss 63× (N.A. 1.4) objective on an Axiovert 35 microscope (Zeiss) with an attached MRC1024 laser scanning confocal microscope system (BioRad). A series of 10 digital images (512 × 512 pixels) of the neuronal cells were obtained. Each digital image contained between 6 and 10 cells. On average, 50 cells were analyzed per condition, with ImageJ program to determine the pixel intensity and particle number inside (intracellular) and around the cells (pericellular). At first, images were converted to grayscale then inverted and a mask generated to segment the two cellular compartments. Then, the region of interest in the cellular compartment was traced semi-automatically and a threshold was applied followed by estimation of pixel intensity and particle counts. Values were expressed as mean ± SEM per image per condition.

Statistical analysis

All experiments were performed blind-coded, and all microscopic evaluations were imaged for four fields per slide. Values in the figures are expressed as means ± SEM. To determine the statistical significance, values were compared by using the one-way ANOVA with *post hoc* Dunnet when comparing the scFV-treated samples to LV-control-treated samples. Additional comparisons were done using Tukey–Krammer or Fisher *post hoc* tests. The differences were considered to be significant if *P*-values were <0.05.

Supplementary Material

Supplementary Material is available at *HMG* online.

Acknowledgements

We thank Ms Kosberg for her technical assistance with viral vectors.

Conflict of Interest statement. None declared.

Funding

This work was supported by grants from the National Institute of Health: AG11385, AG5131, AG18840, AG022074 and NS044233.

References

1. Nakamura, T. and Lipton, S.A. (2009) Cell death: protein misfolding and neurodegenerative diseases. *Apoptosis*, **14**, 455–468.
2. Lee, S.J., Lim, H.S., Masliah, E. and Lee, H.J. (2011) Protein aggregate spreading in neurodegenerative diseases: problems and perspectives. *Neurosci. Res.*, **70**, 339–348.
3. Burre, J., Sharma, M., Tsetsenis, T., Buchman, V., Etherton, M. R. and Sudhof, T.C. (2010) Alpha-synuclein promotes SNARE-complex assembly in vivo and in vitro. *Science*, **329**, 1663–1667.
4. Martin, F.L., Williamson, S.J., Paleologou, K.E., Allsop, D. and El-Agnaf, O.M. (2004) Alpha-synuclein and the pathogenesis of Parkinson's disease. *Protein Pept. Lett.*, **11**, 229–237.
5. Spillantini, M.G., Schmidt, M.L., Lee, V.M., Trojanowski, J.Q., Jakes, R. and Goedert, M. (1997) Alpha-synuclein in Lewy bodies. *Nature*, **388**, 839–840.
6. Lashuel, H.A., Overk, C.R., Oueslati, A. and Masliah, E. (2013) The many faces of alpha-synuclein: from structure and toxicity to therapeutic target. *Nat. Rev. Neurosci.*, **14**, 38–48.
7. Eller, M. and Williams, D.R. (2011) alpha-Synuclein in Parkinson disease and other neurodegenerative disorders. *Clin. Chem. Lab. Med.*, **49**, 403–408.
8. Lee, S.J. (2008) Origins and effects of extracellular alpha-synuclein: implications in Parkinson's disease. *J. Mol. Neurosci.*, **34**, 17–22.
9. Steiner, J.A., Angot, E. and Brundin, P. (2011) A deadly spread: cellular mechanisms of alpha-synuclein transfer. *Cell Death Differ.*, **18**, 1425–1433.
10. Henne, W.M., Stenmark, H. and Emr, S.D. (2013) Molecular mechanisms of the membrane sculpting ESCRT pathway. *Cold Spring Harb. Perspect. Biol.*, **5**, 1–12.
11. Williams, R.L. and Urbe, S. (2007) The emerging shape of the ESCRT machinery. *Nat. Rev. Mol. Cell Biol.*, **8**, 355–368.
12. Wollert, T., Yang, D., Ren, X., Lee, H.H., Im, Y.J. and Hurley, J.H. (2009) The ESCRT machinery at a glance. *J. Cell Sci.*, **122**, 2163–2166.
13. Filimonenko, M., Stuffers, S., Raiborg, C., Yamamoto, A., Malerod, L., Fisher, E.M., Isaacs, A., Brech, A., Stenmark, H. and Simonsen, A. (2007) Functional multivesicular bodies are required for autophagic clearance of protein aggregates associated with neurodegenerative disease. *J. Cell Biol.*, **179**, 485–500.
14. Skibinski, G., Parkinson, N.J., Brown, J.M., Chakrabarti, L., Lloyd, S.L., Hummerich, H., Nielsen, J.E., Hodges, J.R., Spillantini, M.G., Thusgaard, T. *et al.* (2005) Mutations in the endosomal ESCRTIII-complex subunit CHMP2B in frontotemporal dementia. *Nat. Genet.*, **37**, 806–808.
15. Belly, A., Bodon, G., Blot, B., Bouron, A., Sadoul, R. and Goldberg, Y. (2010) CHMP2B mutants linked to frontotemporal dementia impair maturation of dendritic spines. *J. Cell Sci.*, **123**, 2943–2954.
16. Parkinson, N., Ince, P.G., Smith, M.O., Highley, R., Skibinski, G., Andersen, P.M., Morrison, K.E., Pall, H.S., Hardiman, O., Collinge, J. *et al.* (2006) ALS phenotypes with mutations in CHMP2B (charged multivesicular body protein 2B). *Neurology*, **67**, 1074–1077.
17. Cox, L.E., Ferraiuolo, L., Goodall, E.F., Heath, P.R., Higginbottom, A., Mortiboys, H., Hollinger, H.C., Hartley, J.A., Brockington, A., Burness, C.E. *et al.* (2010) Mutations in CHMP2B in lower motor neuron predominant amyotrophic lateral sclerosis (ALS). *PLoS ONE*, **5**, e9872.
18. Hooli, B.V., Kovacs-Vajna, Z.M., Mullin, K., Blumenthal, M.A., Mattheisen, M., Zhang, C., Lange, C., Mohapatra, G., Bertram, L. and Tanzi, R.E. (2014) Rare autosomal copy number variations in early-onset familial Alzheimer's disease. *Mol. Psychiatry*, **19**, 676–681.
19. Lee, J.A., Beigneux, A., Ahmad, S.T., Young, S.G. and Gao, F.B. (2007) ESCRT-III dysfunction causes autophagosome accumulation and neurodegeneration. *Curr. Biol.*, **17**, 1561–1567.
20. Han, J.H., Ryu, H.H., Jun, M.H., Jang, D.J. and Lee, J.A. (2012) The functional analysis of the CHMP2B missense mutation associated with neurodegenerative diseases in the endolysosomal pathway. *Biochem. Biophys. Res. Commun.*, **421**, 544–549.
21. Kim, C., Ho, D.H., Suk, J.E., You, S., Michael, S., Kang, J., Joong Lee, S., Masliah, E., Hwang, D., Lee, H.J. *et al.* (2013) Neuron-released oligomeric alpha-synuclein is an endogenous agonist of TLR2 for paracrine activation of microglia. *Nat. Commun.*, **4**, 1562.
22. Spencer, B., Potkar, R., Trejo, M., Rockenstein, E., Patrick, C., Gindi, R., Adame, A., Wyss-Coray, T. and Masliah, E. (2009) Beclin 1 gene transfer activates autophagy and ameliorates the neurodegenerative pathology in alpha-synuclein models of Parkinson's and Lewy body diseases. *J. Neurosci.*, **29**, 13578–13588.
23. Crews, L., Spencer, B., Desplats, P., Patrick, C., Paulino, A., Rockenstein, E., Hansen, L., Adame, A., Galasko, D. and Masliah, E. (2010) Selective molecular alterations in the autophagy pathway in patients with Lewy body disease and in models of alpha-synucleinopathy. *PLoS ONE*, **5**, e9313.
24. Yamazaki, Y., Takahashi, T., Hiji, M., Kurashige, T., Izumi, Y., Yamawaki, T. and Matsumoto, M. (2010) Immunopositivity for ESCRT-III subunit CHMP2B in granulovacuolar degeneration of neurons in the Alzheimer's disease hippocampus. *Neurosci. Lett.*, **477**, 86–90.
25. Kurashige, T., Takahashi, T., Yamazaki, Y., Hiji, M., Izumi, Y., Yamawaki, T. and Matsumoto, M. (2013) Localization of CHMP2B-immunoreactivity in the brainstem of Lewy body disease. *Neuropathology*, **33**, 237–245.
26. Price, D.L., Rockenstein, E., Ubhi, K., Phung, V., MacLean-Lewis, N., Askay, D., Cartier, A., Spencer, B., Patrick, C., Desplats, P. *et al.* (2010) Alterations in mGluR5 expression and signaling in Lewy body disease and in transgenic models of alpha-synucleinopathy: implications for excitotoxicity. *PLoS ONE*, **5**, e14020.
27. Overk, C.R. and Masliah, E. (2014) Pathogenesis of synaptic degeneration in Alzheimer's disease and Lewy body disease. *Biochem. Pharmacol.*, **88**, 508–516.
28. Magen, I., Fleming, S.M., Zhu, C., Garcia, E.C., Cardiff, K.M., Dinh, D., De La Rosa, K., Sanchez, M., Torres, E.R., Masliah, E. *et al.* (2012) Cognitive deficits in a mouse model of pre-manifest Parkinson's disease. *Eur. J. Neurosci.*, **35**, 870–882.

29. Rajendran, L., Bali, J., Barr, M.M., Court, F.A., Kramer-Albers, E. M., Picou, F., Raposo, G., van der Vos, K.E., van Niel, G., Wang, J. *et al.* (2014) Emerging roles of extracellular vesicles in the nervous system. *J. Neurosci.*, **34**, 15482–15489.
30. Mollenhauer, B., Trautmann, E., Otte, B., Ng, J., Spreer, A., Lange, P., Sixel-Doring, F., Hakimi, M., Vonsattel, J.P., Nussbaum, R. *et al.* (2012) alpha-Synuclein in human cerebrospinal fluid is principally derived from neurons of the central nervous system. *J. Neural Transm.*, **119**, 739–746.
31. Lee, S.J., Desplats, P., Sigurdson, C., Tsigelny, I. and Masliah, E. (2010) Cell-to-cell transmission of non-prion protein aggregates. *Nat. Rev. Neurol.*, **6**, 702–706.
32. Emmanouilidou, E., Melachroinou, K., Roumeliotis, T., Garbis, S.D., Ntzouni, M., Margaritis, L.H., Stefanis, L. and Vekrellis, K. (2010) Cell-produced alpha-synuclein is secreted in a calcium-dependent manner by exosomes and impacts neuronal survival. *J. Neurosci.*, **30**, 6838–6851.
33. Danzer, K.M., Kranich, L.R., Ruf, W.P., Cagsal-Getkin, O., Winslow, A.R., Zhu, L., Vanderburg, C.R. and McLean, P.J. (2012) Exosomal cell-to-cell transmission of alpha synuclein oligomers. *Mol. Neurodegener.*, **7**, 42.
34. Lee, H.J., Suk, J.E., Bae, E.J., Lee, J.H., Paik, S.R. and Lee, S.J. (2008) Assembly-dependent endocytosis and clearance of extracellular alpha-synuclein. *Int. J. Biochem. Cell Biol.*, **40**, 1835–1849.
35. Tsigelny, I.F., Sharikov, Y., Wrasidlo, W., Gonzalez, T., Desplats, P.A., Crews, L., Spencer, B. and Masliah, E. (2012) Role of alpha-synuclein penetration into the membrane in the mechanisms of oligomer pore formation. *FEBS J.*, **279**, 1000–1013.
36. Pfefferkorn, C.M., Heinrich, F., Sodt, A.J., Maltsev, A.S., Pastor, R.W. and Lee, J.C. (2012) Depth of alpha-synuclein in a bilayer determined by fluorescence, neutron reflectometry, and computation. *Biophys. J.*, **102**, 613–621.
37. Wietek, J., Haralampiev, I., Amoussouvi, A., Herrmann, A. and Stockl, M. (2013) Membrane bound alpha-synuclein is fully embedded in the lipid bilayer while segments with higher flexibility remain. *FEBS Lett.*, **587**, 2572–2577.
38. Chai, Y.J., Kim, D., Park, J., Zhao, H., Lee, S.J. and Chang, S. (2013) The secreted oligomeric form of alpha-synuclein affects multiple steps of membrane trafficking. *FEBS Lett.*, **587**, 452–459.
39. Lopes da Fonseca, T., Villar-Pique, A. and Outeiro, T.F. (2015) The interplay between alpha-synuclein clearance and spreading. *Biomolecules*, **5**, 435–471.
40. Teis, D., Saksena, S. and Emr, S.D. (2008) Ordered assembly of the ESCRT-III complex on endosomes is required to sequester cargo during MVB formation. *Dev. Cell*, **15**, 578–589.
41. Lee, J.A., Liu, L., Javier, R., Kreitzer, A.C., Delaloy, C. and Gao, F.B. (2011) ESCRT-III subunits Snf7-1 and Snf7-2 differentially regulate transmembrane cargos in hESC-derived human neurons. *Mol. Brain*, **4**, 37.
42. Henne, W.M., Buchkovich, N.J. and Emr, S.D. (2011) The ESCRT pathway. *Dev. Cell*, **21**, 77–91.
43. Stuchell-Brereton, M.D., Skalicky, J.J., Kieffer, C., Karren, M.A., Ghaffarian, S. and Sundquist, W.I. (2007) ESCRT-III recognition by VPS4 ATPases. *Nature*, **449**, 740–744.
44. Freeman, D., Cedillos, R., Choyke, S., Lukic, Z., McGuire, K., Marvin, S., Burrage, A.M., Sudholt, S., Rana, A., O'Connor, C. *et al.* (2013) Alpha-synuclein induces lysosomal rupture and cathepsin dependent reactive oxygen species following endocytosis. *PLoS ONE*, **8**, e62143.
45. Braak, H. and Braak, E. (2000) Pathoanatomy of Parkinson's disease. *J. Neurol.*, **247**(Suppl 2), II3–I10.
46. Marxreiter, F., Ettle, B., May, V.E., Esmer, H., Patrick, C., Kragh, C.L., Klucken, J., Winner, B., Riess, O., Winkler, J. *et al.* (2013) Glial A30P alpha-synuclein pathology segregates neurogenesis from anxiety-related behavior in conditional transgenic mice. *Neurobiol. Dis.*, **59**, 38–51.
47. Rey, N.L., Petit, G.H., Bousset, L., Melki, R. and Brundin, P. (2013) Transfer of human alpha-synuclein from the olfactory bulb to interconnected brain regions in mice. *Acta Neuropathol.*, **126**, 555–573.
48. Xilouri, M., Vogiatzi, T., Vekrellis, K., Park, D. and Stefanis, L. (2009) Abberant alpha-synuclein confers toxicity to neurons in part through inhibition of chaperone-mediated autophagy. *PLoS ONE*, **4**, e5515.
49. Cuervo, A.M., Stefanis, L., Fredenburg, R., Lansbury, P.T. and Sulzer, D. (2004) Impaired degradation of mutant alpha-synuclein by chaperone-mediated autophagy. *Science*, **305**, 1292–1295.
50. Lee, H.J., Cho, E.D., Lee, K.W., Kim, J.H., Cho, S.G. and Lee, S.J. (2013) Autophagic failure promotes the exocytosis and intercellular transfer of alpha-synuclein. *Exp. Mol. Med.*, **45**, e22.
51. Tanikawa, S., Mori, F., Tanji, K., Kakita, A., Takahashi, H. and Wakabayashi, K. (2012) Endosomal sorting related protein CHMP2B is localized in Lewy bodies and glial cytoplasmic inclusions in alpha-synucleinopathy. *Neurosci. Lett.*, **527**, 16–21.
52. Isaacs, A.M., Johannsen, P., Holm, I. and Nielsen, J.E. and consortium, F.R. (2011) Frontotemporal dementia caused by CHMP2B mutations. *Curr. Alzheimer Res.*, **8**, 246–251.
53. Cannon, A., Baker, M., Boeve, B., Josephs, K., Knopman, D., Petersen, R., Parisi, J., Dickison, D., Adamson, J., Snowden, J. *et al.* (2006) CHMP2B mutations are not a common cause of frontotemporal lobar degeneration. *Neurosci. Lett.*, **398**, 83–84.
54. Rizzu, P., van Mil, S.E., Anar, B., Rosso, S.M., Donker Kaat, L., Heutink, P. and van Swieten, J.C. (2006) CHMP2B mutations are not a cause of dementia in Dutch patients with familial and sporadic frontotemporal dementia. *Am. J. Med. Genet. B, Neuropsychiatr. Genet.*, **141B**, 944–946.
55. Gascon, E., Lynch, K., Ruan, H., Almeida, S., Verheyden, J.M., Seeley, W.W., Dickson, D.W., Petrucelli, L., Sun, D., Jiao, J. *et al.* (2014) Alterations in microRNA-124 and AMPA receptors contribute to social behavioral deficits in frontotemporal dementia. *Nat. Med.*, **20**, 1444–1451.
56. Ghazi-Noori, S., Froud, K.E., Mizielinska, S., Powell, C., Smidak, M., Fernandez de Marco, M., O'Malley, C., Farmer, M., Parkinson, N., Fisher, E.M. *et al.* (2012) Progressive neuronal inclusion formation and axonal degeneration in CHMP2B mutant transgenic mice. *Brain*, **135**, 819–832.
57. Nielsen, T.T., Mizielinska, S., Hasholt, L., Isaacs, A.M., Nielsen, J.E. and Consortium, F.R. (2012) Reversal of pathology in CHMP2B-mediated frontotemporal dementia patient cells using RNA interference. *J. Gene Med.*, **14**, 521–529.
58. Rascovsky, K., Salmon, D.P., Ho, G.J., Galasko, D., Peavy, G.M., Hansen, L.A. and Thal, L.J. (2002) Cognitive profiles differ in autopsy-confirmed frontotemporal dementia and AD. *Neurology*, **58**, 1801–1808.
59. Hansen, L., Salmon, D., Galasko, D., Masliah, E., Katzman, R., DeTeresa, R., Thal, L., Pay, M.M., Hofstetter, R., Klauber, M. *et al.* (1990) The Lewy body variant of Alzheimer's disease: a clinical and pathologic entity. *Neurology*, **40**, 1–8.
60. Hansen, L.A. (1997) The Lewy body variant of Alzheimer disease. *J. Neural Transm. Suppl.*, **51**, 83–93.
61. Galasko, D., Katzman, R., Salmon, D.P. and Hansen, L. (1996) Clinical and neuropathological findings in Lewy body dementias. *Brain Cogn.*, **31**, 166–175.

62. McKeith, I.G., Galasko, D., Kosaka, K., Perry, E.K., Dickson, D. W., Hansen, L.A., Salmon, D.P., Lowe, J., Mirra, S.S., Byrne, E. J. *et al.* (1996) Consensus guidelines for the clinical and pathologic diagnosis of dementia with Lewy bodies (DLB): report of the consortium on DLB international workshop. *Neurology*, **47**, 1113–1124.
63. Lee, J.A. and Gao, F.B. (2009) Inhibition of autophagy induction delays neuronal cell loss caused by dysfunctional ESCRT-III in frontotemporal dementia. *J. Neurosci.*, **29**, 8506–8511.
64. Bar-On, P., Crews, L., Koob, A.O., Mizuno, H., Adame, A., Spencer, B. and Masliah, E. (2008) Statins reduce neuronal alpha-synuclein aggregation in *in vitro* models of Parkinson's disease. *J. Neurochem.*, **105**, 1656–1667.
65. Lee, S.J., Desplats, P., Lee, H.J., Spencer, B. and Masliah, E. (2012) Cell-to-cell transmission of alpha-synuclein aggregates. *Methods Mol. Biol.*, **849**, 347–359.
66. Tiscornia, G., Singer, O. and Verma, I.M. (2006) Production and purification of lentiviral vectors. *Nat. Protoc.*, **1**, 241–245.
67. Hashimoto, M. and Masliah, E. (2003) Cycles of aberrant synaptic sprouting and neurodegeneration in Alzheimer's and dementia with Lewy bodies. *Neurochem. Res.*, **28**, 1743–1756.
68. Macia, E., Ehrlich, M., Massol, R., Boucrot, E., Brunner, C. and Kirchhausen, T. (2006) Dynasore, a cell-permeable inhibitor of dynamin. *Dev. Cell*, **10**, 839–850.
69. Desplats, P.A., Kass, K.E., Gilmartin, T., Stanwood, G.D., Woodward, E.L., Head, S.R., Sutcliffe, J.G. and Thomas, E.A. (2006) Selective deficits in the expression of striatal-enriched mRNAs in Huntington's disease. *J. Neurochem.*, **96**, 743–757.
70. Perez-Gonzalez, R., Gauthier, S.A., Kumar, A. and Levy, E. (2012) The exosome secretory pathway transports amyloid precursor protein carboxyl-terminal fragments from the cell into the brain extracellular space. *J. Biol. Chem.*, **287**, 43108–43115.
71. Rockenstein, E., Mallory, M., Hashimoto, M., Song, D., Shults, C.W., Lang, I. and Masliah, E. (2002) Differential neuropathological alterations in transgenic mice expressing alpha-synuclein from the platelet-derived growth factor and Thy-1 promoters. *J. Neurosci. Res.*, **68**, 568–578.
72. Games, D., Seubert, P., Rockenstein, E., Patrick, C., Trejo, M., Ubhi, K., Ettle, B., Ghassemiam, M., Barbour, R., Schenk, D. *et al.* (2013) Axonopathy in an alpha-synuclein transgenic model of Lewy body disease is associated with extensive accumulation of C-terminal-truncated alpha-synuclein. *Am. J. Pathol.*, **182**, 940–953.
73. Marr, R.A., Guan, H., Rockenstein, E., Kindy, M., Gage, F.H., Verma, I., Masliah, E. and Hersh, L.B. (2004) Neprilysin regulates amyloid Beta peptide levels. *J. Mol. Neurosci.*, **22**, 5–11.
74. Baekelandt, V., Claeys, A., Eggermont, K., Lauwers, E., De Strooper, B., Nuttin, B. and Debyser, Z. (2002) Characterization of lentiviral vector-mediated gene transfer in adult mouse brain. *Hum. Gene Ther.*, **13**, 841–853.
75. Spencer, B., Marr, R.A., Rockenstein, E., Crews, L., Adame, A., Potkar, R., Patrick, C., Gage, F.H., Verma, I.M. and Masliah, E. (2008) Long-term neprilysin gene transfer is associated with reduced levels of intracellular Abeta and behavioral improvement in APP transgenic mice. *BMC Neurosci.*, **9**, 109.
76. Chen, Y., Huang, X., Zhang, Y.W., Rockenstein, E., Bu, G., Golde, T.E., Masliah, E. and Xu, H. (2012) Alzheimer's beta-secretase (BACE1) regulates the cAMP/PKA/CREB pathway independently of beta-amyloid. *J. Neurosci.*, **32**, 11390–11395.
77. Crews, L., Mizuno, H., Desplats, P., Rockenstein, E., Adame, A., Patrick, C., Winner, B., Winkler, J. and Masliah, E. (2008) Alpha-synuclein alters Notch-1 expression and neurogenesis in mouse embryonic stem cells and in the hippocampus of transgenic mice. *J. Neurosci.*, **28**, 4250–4260.
78. Masliah, E., Rockenstein, E., Veinbergs, I., Mallory, M., Hashimoto, M., Takeda, A., Sagara, Y., Sisk, A. and Mucke, L. (2000) Dopaminergic loss and inclusion body formation in alpha-synuclein mice: implications for neurodegenerative disorders. *Science*, **287**, 1265–1269.
79. Rockenstein, E., Mante, M., Alford, M., Adame, A., Crews, L., Hashimoto, M., Esposito, L., Mucke, L. and Masliah, E. (2005) High beta-secretase activity elicits neurodegeneration in transgenic mice despite reductions in amyloid-beta levels: implications for the treatment of Alzheimer disease. *J. Biol. Chem.*, **280**, 32957–32967.
80. Rockenstein, E., Schwach, G., Ingolic, E., Adame, A., Crews, L., Mante, M., Pfragner, R., Schreiner, E., Windisch, M. and Masliah, E. (2005) Lysosomal pathology associated with alpha-synuclein accumulation in transgenic models using an eGFP fusion protein. *J. Neurosci. Res.*, **80**, 247–259.
81. Mucke, L., Abraham, C., Ruppe, M., Rockenstein, E., Toggas, S., Alford, M. and Masliah, E. (1995) Protection against HIV-1 gp120-induced brain damage by neuronal overexpression of human amyloid precursor protein (hAPP). *J. Exp. Med.*, **181**, 1551–1556.
82. Toggas, S.M., Masliah, E., Rockenstein, E.M., Rall, G.F., Abraham, C.R. and Mucke, L. (1994) Central nervous system damage produced by expression of the HIV-1 coat protein gp120 in transgenic mice. *Nature*, **367**, 188–193.
83. Masliah, E., Rockenstein, E., Mante, M., Crews, L., Spencer, B., Adame, A., Patrick, C., Trejo, M., Ubhi, K., Rohn, T.T. *et al.* (2011) Passive immunization reduces behavioral and neuropathological deficits in an alpha-synuclein transgenic model of Lewy body disease. *PLoS ONE*, **6**, e19338.
84. Rockenstein, E., Mallory, M., Mante, M., Sisk, A. and Masliah, E. (2001) Early formation of mature amyloid-b proteins deposits in a mutant APP transgenic model depends on levels of Ab1-42. *J. Neurosci. Res.*, **66**, 573–582.